Title: Loss of ERK1/2 in the retinal pigment epithelium leads to RPE65 decrease and retinal degeneration.

Pyakurel Aswin[1,2,#], Balmer Delphine[2,#], Saba-El-Leil Marc K.[4], Kizilyaprak Caroline[5], Daraspe Jean[5], Humbel Bruno M.[5], Voisin Laure[4], Le Yun Z.[3], von Lintig Johannes[6], Meloche Sylvain[4] and Roduit Raphaël[1,2,*]

Affiliations:

[1]Department of Ophthalmology, University of Lausanne, Jules-Gonin Eye Hospital, Fondation Asile des Aveugles, 1000 Lausanne, Switzerland. [2]IRO, Institute for Research in Ophthalmology, 1950 Sion, Switzerland. [3]Department of Medicine Endocrinology and Harold Hamm Diabetes Center, University of Oklahoma Health Sciences Center, Oklahoma City, Oklahoma OK 73104, USA. [4]Institute for Research in Immunology and Cancer, Department of Pharmacology and Program of Molecular Biology, Université de Montréal, Montreal H3T 1J4, Quebec, Canada. [5]Electron Microscopy Facility**,** University of Lausanne, 1015 Lausanne, Switzerland. [6]Department of Pharmacology, School of Medicine, Case Western Reserve University, Cleveland OH44106, Ohio, USA.

Running title: ERK1/2 and retinal degeneration

[#] P.A. and B.D contributed equally to the study

* To whom correspondence should be addressed: Raphaël Roduit, Jules-Gonin Eye Hospital, Fondation Asile des Aveugles**,** Group “Macular Degeneration and Diabetic Retinopathy”, Av de France 15**,** CH-1002 Lausanne, raphael.roduit@fa2.ch

Word Count: Abstract: 160 words

Abstract/Introduction/Results/Discussion/FigLeg: 33’682 characters

Abstract

Recent work has suggested that the activity of extracellular signal-regulated kinase (ERK) 1/2 is increased in the retinal pigment epithelium (RPE) of age-related macular degeneration (ARMD) patients and therefore could be an attractive therapeutic target. Notably, ERK1/2 pathway inhibitors are used in cancer therapy, with severe and non-characterized ocular side effects. To decipher the role of ERK1/2 in RPE cells, we conditionally disrupted the *Erk1* and *Erk2* genes in the mouse RPE. Loss of ERK1/2 activity resulted in a significant decrease of RPE65 expression, a decrease in ocular retinoid levels concomitant with low visual function and a rapid disorganization of RPE cells, ultimately leading to retinal degeneration. Our results identify the ERK1/2 pathway as a direct regulator of the visual cycle and a critical component for the viability of RPE and photoreceptor cells. Moreover, they caution about the need for a very fine adjustment of kinase inhibition in cancer or ARMD treatment in order to avoid the ocular side effects.

Introduction

ARMD is the most common cause of blindness in individuals over 50 years of age. This pathology is characterized by the presence of soft and/or hard drusen (extracellular debris and deposits), hyper- and hypo-pigmentation of retinal pigment epithelium (RPE) cells, RPE and photoreceptor apoptosis as well as choroidal neovascularization (CNV) (1). Two subgroups of ARMD can be distinguished: the dry form (geographic atrophy, GA) and the wet form (exudative). The dry form is characterized by the formation of drusen between RPE cells and Bruch's membrane (2). This accumulation is toxic for RPE cells, altering some of their important functions. The wet form is linked to CNV affecting the subretinal macular region, which eventually results in a loss of central vision.

An accumulation of intracellular lipofuscin occurs in both forms of ARMD. One of the major components of lipofuscin is the retinoid derivative, N-retinyl-N-retinylidene

ethanolamine (A2E). A2E has a broad light absorption spectrum, with a peak in the blue range (~430nm). Therefore, it is a potent photo-inducible generator of reactive oxygen species (ROS) which can damage proteins, lipids and DNA of RPE cells (3-5). Even if new imaging techniques did not reveal any correlation between A2E distribution and lipofuscin fluorescence in human RPE (6), it remains unclear whether metabolites or modified forms of A2E could be deleterious for the retina and RPE; especially because A2E accumulation is linked to lipofuscin increase with age (7). Moreover, the accumulation of A2E in phagolysosomes can lead to inhibition of the turnover of endogenous proteins in cultured RPE cells by abolishing the pH gradient required for the normal function of these organelles (8). This damage leads to apoptosis and impaired RPE cell functions. In addition, previous work from our laboratory showed that A2E induces a strong decrease in extracellular signal-regulated kinase (ERK) 1/2 activity in polarized ARPE19 and isolated mouse RPE cells, and inhibition of ERK1/2 leads to a significant decrease of retinal pigment epithelium-specific protein 65kDa (RPE65) (9).

Mitogen-activated protein kinases (MAPKs) are evolutionarily conserved protein kinases that transduce signals to regulate gene expression during cell proliferation, survival and differentiation (10-12). There are two different groups of MAPKs: the conventional (ERK1/2/5, p38 kinases and JNK1/2/3) and the atypical (ERK3/4, ERK7 and NLK) MAPKs (13). Due to their important roles in cellular homeostasis, abnormal regulation of the conventional MAPK pathways has been linked to a wide range of diseases (12, 14-17). The ERK1/2 pathway in particular is commonly deregulated in human cancer, which has led to the development and clinical evaluation of several small molecule inhibitors targeting components of this pathway (18, 19). Notably, the clinical benefit of these molecules is limited by mechanism-based side effects of blurred vision and altered light perception (20, 21).

Growing evidence indicates an important role of ERK1/2 signaling in retinal function. Retina maturation is associated with the activation of ERK1/2, which are proposed to play a survival role during development (22). We recently showed that ERK1/2 activity is upregulated in RPE65-KO mice (23) and is decreased when ARPE19 cells are exposed to UV stress (24). Regeneration of the chick embryo retina was found to associated with FGF/FGFR/MEK/ERK-dependent upregulation of the paired homeobox transcription factor PAX6 in the RPE (25). Interestingly, recent clinical studies by the group of Ambati revealed the increase of ERK1/2 activity in the RPE of patients suffering from GA as well as in a mouse model of RPE degeneration induced by DICER1 depletion (26). These findings suggest a key role for ERK1/2 in ARMD and support the concept of ERK1/2 inhibition as a possible treatment of the disease (26). However, the ERK1/2 signaling pathway is complex, with multiple roles in differentiation,proliferation and cell death pathways depending on the cellular context. This complexity has been described in many studies (27, 28) and is a central question in order to understand the role of these kinases before considering to modulate its activity for therapeutic purposes.

Inhibitors of the ERK1/2 pathway used in cancer therapy may provoke ocular secondary effects (21), yet this treatment is proposed for ARMD (26). In fact, little is known about the real impact of blocking these kinases in the mouse retina. Therefore, in order to obtain valuable insights about ERK1/2 inhibition and to understand the role of ERK1/2 signaling in the maintenance and survival of RPE cells, we established a mouse line with an RPE-specific knockout of *Erk1* and *Erk2* genes (RPE-DKO). Fundus analyses of mice with RPE-specific loss of ERK1/2 showed macular depigmentation. Electroretinogram (ERG) analyses combined with retinoid measurements revealed dysfunctional vision as well as a significant decrease in the ocular retinoids content. Optical coherence tomography (OCT) analyses confirmed the retinal structure disorganization and immunohistochemical

analyses demonstrated RPE morphology alteration and consequent photoreceptor (PR) loss. At the onset of retinal degeneration, loss of ERK1/2 led to the specific decrease of RPE65 with mislocalization of lecithin retinol acyltransferase (LRAT). The diminution of RPE65 expression depended on the presence of an AP-1 site in the promoter region, as cFOS and FRA-1 (Fos Related Antigen – 1) protein expression is decreased and binding to this AP-1 site reduced in RPE-DKO mice.

Results

RPE-specific loss of ERK1/2 causes vision impairment due to the deficit of retinoids.

In order to establish a mouse line with an RPE-specific knockout of *Erk1* and *Erk2* genes, we used *Erk1*$^{-/-}$ mice with a conditional allele of *Erk2* (*Erk1*$^{-/-}$;*Erk2*$^{f/f}$) (29) crossed with transgenic mice carrying the human vitelliform macular dystrophy-2 (VMD2) promoter-directed reverse tetracycline-dependent transactivator (rtTA) and the tetracycline-responsive element (TRE)-directed Cre (VMD2-rtTA/TRE-Cre) (30), called RPE-Cre, to obtain *VMD2-rtTA/TRE-Cre;Erk1*$^{-/-}$;*Erk2*$^{f/f}$ mice. Doxycycline treatment of these mice leads to the disruption of *Erk2* specifically in RPE cells. The *VMD2-rtTA/TRE-Cre;Erk1*$^{-/-}$;*Erk2*$^{\Delta/\Delta}$ (RPE-DKO) line was then compared to *Erk1*$^{-/-}$;*Erk2*$^{f/f}$ as control mice (CTL).

We first analyzed the visual function and retinal structure of RPE-DKO mice in comparison to CTL mice. Doxycycline (Dox)-induced expression of Cre in RPE cells was verified by crossing RPE-Cre animals with tdTomato mice (31) to generate RPE-Cre-tdTomato mice. Two intraperitoneal (IP) injections of 10 µg Dox, one week apart, at 2 months of age triggered consistent expression of Cre specifically in RPE cells (Fig. 1A). This protocol was followed to induce Cre protein expression in 2 month-old RPE-DKO mice, while 2 month-old CTL mice were injected with PBS. The genotypes of all mice were confirmed by PCR amplification of *Cre*, *Erk1* KO and *Erk2* floxed alleles (Fig. 1B and C); deletion of *Erk2* in RPE was confirmed by the analysis of RPE genomic DNA as evidenced by the presence of the delta (Δ) band (Fig. 1D).

Immunostaining shows the decrease of ERK2 in RPE of RPE-DKO at 1 month in comparison to control mice (Fig. 1E). In addition, Western Blot analysis of RPE protein lysates clearly shows the absence of ERK1 in both RPE-DKO and CTL mice and the decrease of ERK2 only in RPE-DKO mouse (Fig. 1F). The fundus analysis showed apparent depigmentation of RPE-DKO eyes (Fig. 2A). OCT analyses performed on RPE-DKO at 4 months, revealed degeneration of the retina with a significant reduction of all retinal and choroidal layers (Fig. 2B). In accordance with this result, ERG analyses revealed a significant impairment of vision in RPE-DKO at 2 months, as revealed by the lower amplitude of the b wave in both the scotopic and photopic stimulations (Fig. 2C). Scotopic patterns (50 mcd s/m2) demonstrated the absence or severe reduction of a and b waves in RPE-DKO mice in comparison to CTL mice, while photopic patterns (10 mcd s/m2) showed an absence of stimulation in RPE-DKO mice (Fig. 2C, right panel). This clearly indicates impairment in both the cone and the rod photoreceptor responses to light stimuli in RPE-DKO animals.

The severe vision damage and retinal degeneration observed in RPE-DKO mice led us to measure the relative amounts of visual cycle intermediates. Mice that had been dark-adapted for 12 h were enucleated under dim light. The retina was separated from the choroid and subjected to HPLC analyses as previously described (32). Loss of ERK1/2 in the RPE led to a significant decrease of ocular retinoids. Retinyl esters in the choroid (dissected including the RPE cells) were significantly reduced. In the retina of dark-adapted eyes, a decrease of more than half of the 11-*cis*-retinal and all-*trans*-retinal was observed (Fig. 2D). We further intended to measure how light influences the ocular retinoid composition of these mice. Thus, we exposed them to bright light where the turnover of visual cycle is enhanced. As expected, we observed an increase of all-*trans*-retinol and retinyl ester(s) after light treatment. Notably, both retinoids were significantly lower in RPE-DKO mice when compared to controls, indicating an impairment of the visual cycle in both dark-adapted and light-exposed

mice (Fig. 2D). We also noted, by immunostaining analysis, a decrease in the expression of stimulated by retinoic acid 6 (STRA6) protein, the membrane receptor for retinol binding protein found in the RPE in RPE-DKO at 1 month (data not shown). This decrease suggests that a reduction of retinoid uptake from the circulation could contribute to the diminished ocular retinoid levels in RPE-DKO mice.

RPE-specific loss of ERK1/2 causes a significant thinning of ONL/INL layers

Visual impairment along with retinal dysfunction led us to examine the photoreceptor structure in RPE-DKO mice. Staining with various cone and rod markers was performed to analyze the integrity of the distinct retinal layers. Retinal degeneration was only observed in RPE-DKO mice; as controls, we used ERK1-/-;Erk2f/f mice treated with PBS (CTL), ERK1-/-;Erk2f/f mice treated with Dox and VMD2-rtTA/TRE-Cre;ERK1-/-;Erk2f/f treated with PBS; none of these mice showed retinal degeneration (data not shown). No toxic effect of Dox was observed in CTL (data not shown) or in Cre-tdTomato (Fig. 1A). RPE-DKO mice exhibited a reduction of cone markers as well as of the outer nuclear layer (ONL) and the inner nuclear layer (INL) thicknesses. Levels of CONE ARRESTIN and GNAT2 showed a marked decrease in RPE-DKO mice at 2 months, and this effect was more pronounced at 4 months (Fig. 3A). The important loss of cone markers occurred before the disappearance of respective rod markers as shown by immunostaining of GNAT2 (Fig. 3A and B). The rod markers RHODOPSIN and GNAT1 were slightly decreased in RPE-DKO mice, principally in the ONL. In addition, the outer segment (OS) length is already smaller in RPE-DKO at 2 months (Fig. 3A). Retinal degeneration could explain the absence of marked reduction of GNAT1 protein expression shown by Western Blot analysis, because both GNAT1 and TUBULIN are decreased, so the ratio is not changed. Measurement of the thickness of ONL and INL layers confirmed a clear decrease in both cases underlining the devastating effect of ERK1**/**2 loss in RPE cells (Fig. 3C). In fact, ONL and INL thickness were reduced by 50 % after only two months of

ERK1/2 loss and by up to 70 % after 4 months (Fig. 3C). We found staining of both GNAT1 and CONE-ARRESTIN in RPE of RPE-DKO at 1 month, while no staining was observed in RPE of control (CTL) mice, as expected (Fig. 3D); this information supports the hypothesis of a defect in phagocytosis process in these mice. Interestingly, ONL and INL degenerations correlated with the a level of cell death as demonstrated by TUNEL assays performed on RPE-DKO and CTL mice (Fig. 3E). The decrease of the ONL and outer segment (OS) thickness as well as the structural disorganization of the entire retina was confirmed by electron microscopy (EM) imaging, revealing the disruption of the inner segment (IS) and OS of photoreceptor cells (Fig. 4A). This disruption and loss of the OS in particular were quantified by measuring the ONL, OS and IS lengths (Fig. 4B). A follow-up study of the mice for one year showed the disappearance of the ONL and a drastic thinning of the INL layer, with no staining for cones or rods. The only persisting staining was GFAP in the ganglion cell layer (GCL) and glycine in the inner plexiform layer (IPL) (Fig. 4C).

RPE-specific loss of ERK1/2 causes specific reduction in cone markers

Additional biochemical analyses were carried out in order to verify the loss of cone photoreceptors. Western blot analysis of retinas from the CTL and RPE-DKO mice showed that GNAT2, a specific cone marker, was significantly reduced at 2 months and by more than 60 % at 4 months (Fig. 5A). However, at 4 months, we observed a marked decrease in both the ONL and INL thickness, which could not only be due to cone photoreceptor loss. Indeed, at 2 months, the level of GNAT1 is already slightly affected, while at 4 months the difference is visible even if not significant. At 4 months, the decrease of photoreceptor proteins was mirrored by a reduction in their mRNA levels. Quantitative PCR (QPCR) showed that specific cone markers, including *Gnat2*, *ConeArrestin*, *mOpsin* and *sOpsin* were significantly lowered at 2 months and decreased further by 60-80% at 4 months (Fig. 5B). In agreement with Western blot studies, the specific rod markers *Gnat1* and *Rho* showed no difference

at 2 months, but declined at 4 months albeit the reduction was not statistically significant. Retinal degeneration could explain the absence of significant reduction of GNAT1 protein expression showed by Western Blot, because both GNAT1 and TUBULIN are decreased, so the ratio is not changed.

Loss of ERK1/2 in RPE causes RPE ultrastructural damage

Loss of vision as well as pronounced retinal degeneration in these mice prompted us to examine the state of the RPE ultrastructure in RPE-DKO at 1 month by EM imaging. An overview of the RPE/retina cell layers showed massive shrinking of the RPE cell layer, disruption of the Bruch's membrane (BM) and photoreceptor (PR) degeneration (Fig. 6A). In order to characterize the damage to the RPE/retinal layer in more detail, different layers were observed separately and quantified. The BM ultrastructure was clearly disrupted and the thickness of the membrane was significantly reduced (Fig. 6B). The RPE cell layer exhibited massive shrinkage as evidenced by the significant reduction of its length (Fig. 6C). The ultrastructural damage of the RPE cell layer was accompanied by the accumulation of mitochondria at the basolateral layer membrane as demonstrated by the significant increase of the organelles area when normalized to the area of cytosol (Fig. 6C). The RPE cell layer of RPE-DKO mice contained structures enriched in membranes which resembled phagolysosomes of the OS of PR (Fig. 6D). This indicates that phagocytosis of OS, one of the major functions of RPE cells, is impaired in RPE-DKO mice. Confirmation was obtained by the presence of GNAT1 and CONE-ARRESTIN in the RPE of RPE-DKO at 1 month (Fig. 3D). Ultrastructural analysis demonstrated that the RPE-specific loss of ERK1/2 caused massive alterations to the ultrastructure not only of the RPE cell layer but also of the BM and the retinal cell layer. The ultrastructural RPE damage in RPE-DKO mice was confirmed by flatmount RPE-choroid analysis. Phalloidin staining revealed a disorganized RPE structure along with increased RPE

cell size including multinucleated cells (Fig. 6E). Total loss of RPE cells was observed in parts of the retina of RPE-DKO at 2 months (Fig. 6F).

ERK1/2 directly regulate RPE65 levels

We previously showed that inhibition of the ERK1/2 pathway in ARPE19 as well as in isolated mouse RPE cells leads to a reduction of *Rpe65* mRNA expression (9). This decrease was confirmed by RPE65 immunostaining in RPE-DKO at 1 month or at 2 weeks respectively (Fig. 7A and B). In addition, we observed a mislocalization of LRAT, the enzyme upstream of RPE65 in the visual cycle, to the apical side of the RPE cells in RPE-DKO mice instead of the basolateral side as observed in CTL mice (Fig. 7A and B). QPCR analysis confirmed the results of immunostaining and revealed that RPE65 but not LRAT expression was significantly decreased in the RPE cells of RPE-DKO at 1 month (Fig. 7C). RPE65 protein expression, normalized by TUBULIN, is significantly reduced in RPE-DKO at 1 month (Fig. 7D). Notably, the promoter of *RPE65* has been shown to contain an AP-1 site, which is under transcriptional control by the AP-1 family of proteins (33). We thus carried out an *in vitro* luciferase reporter assay using RPE65 (33) or LRAT (34) promoter constructs. Luciferase activity was detected with both promoters transfected into the HEK293 cell line (Fig. 7E). Treatment with the MEK1/2 inhibitor U0126 caused a significant decrease of the activity of the RPE65 promoter, while no change in activity was observed when the luciferase reporter is driven by LRAT promoter. Addition of U0126 did not significantly affect the luciferase activity when the AP-1 site in the *RPE65* promoter reporter construct was deleted, indicating that it is mandatory for the regulation by ERK1/2. Next, we set out to identify the downstream effectors of ERK1/2 that regulate this AP-1 site. Nuclear proteins of ARPE19 cells showed a strong binding to the AP-1 sequence which was reduced in the presence of a competitor AP-1 oligonucleotide as well as by treatment with U0126 (Fig. 7F). In order to identify which factors regulated by ERK1/2 are part of the AP-1 complex,

nuclear extracts from ARPE19 cells were subjected to an AP-1 ELISA binding assay that included individual AP-1 family transcription factors. Inhibition of the ERK1/2 pathway in ARPE19 cells, using either U0126 or PD0325901, led to a decrease of c-FOS and FRA-1 protein binding to the AP-1 sequence (Fig. 7F), whereas the inhibitors had no effect on c-JUN, JUN-B and JUN-D binding (data not shown). In order to investigate whether this effect is maintained in the RPE-DKO mice, whole cell protein lysates from isolated RPE cells were subjected to an AP-1 DNA-binding assay. Indeed, the binding of C-FOS and FRA-1 to AP-1 was significantly reduced (Fig. 7G) and C-FOS and FRA-1 protein expressions were decreased in RPE of RPE-DKO mice at 1 month (Fig. 7G). Taken together, the analyses in cell culture and in the mouse model argue in favor of a direct regulation of *RPE65* gene expression by the ERK1/2 pathway via the binding of C-FOS and FRA-1 complexes to the AP-1 site in the upstream promoter region.

Discussion

In order to evaluate the potential use of ERK1/2 pathway inhibitors in ARMD treatment and to better understand the ocular side effects observed in cancer patients treated with such inhibitors, we disrupted ERK1/2 expression specifically in RPE cells of the mouse. We observed two major consequences: First, the down-regulation of RPE65, the mislocalization of LRAT and the depletion of the retinoid content. This already occurrs 1 month after ERK1/2 depletion, when retinal degeneration just begins to be detected, as shown by chromatin compaction in ONL cells as well as shortening of photoreceptor OS. Second, changes in the morphology of the RPE and in the RPE cell death process, which appears later, two months after Cre induction, when most of the hallmarks of retinal degeneration are visible in the eyes of RPE-DKO mice.

RPE65 is an enzyme involved in vitamin A metabolism in RPE cells (35). This key protein of the visual cycle catalyzes the transformation of all-*trans* retinyl to 11-cis

retinol. Mutations in RPE65 are associated with several retinal disorders including Retinitis Pigmentosa (RP), Leber Congenital Amaurosis (LCA) (36) and early onset retinal dystrophy (RD) in children (37). Much effort has been devoted to deciphering the roles of various genetic mutations that are linked to these diseases (38). However, little is known about how the activity of RPE65 is regulated at the RPE cell level. Several studies analyzed the promoter region of the *RPE65* gene (33, 39) but little is known about the factors involved in its transcriptional regulation. Retinoic acid has been suggested to participate to the down-regulation of *RPE65* (40) as well as of fatty acid transporter protein 4 (FATP4) and to the elongation of very long chain fatty acid protein 1 (ELOVL1) (41). Recently, Masuda and colleagues provided evidence for an involvement of the sex-determining region Y box containing-gene 9 (SOX9) in the regulation of the transcription of visual cycle genes, including RPE65, retinaldehyde binding protein 1 (RBP-1) and retinal G protein-coupled receptor (RGR). They showed that SOX9 acts synergistically with orthodenticle homeobox 2 (OTX2) to activate *RPE65* gene expression (42). Here we identify another critical upstream regulatory factor for *RPE65*. We demonstrate that the disruption of ERK1/2 specifically in RPE cells leads to a marked decrease of *RPE65* expression that occurs through an AP-1 site present in the promoter region of the *RPE65* gene. The inhibitory effect of U0126 on reporter gene expression was completely abrogated when the AP-1 site was removed, even if we cannot exclude that other regulatory elements close to the AP-1 sequence were also deleted from the construct; this could explain the low promoter activity observed in absence of AP-1 sequence. The key roles of cFOS and FRA-1 were confirmed by western blot analysis and by a DNA AP-1 binding assay. Interestingly, ERK1/2 and SOX9 signaling pathways have been recently shown to interact in urothelial carcinoma (43) and zebrafish sex determination (44). Moreover, activation of ERK1/2 is associated with an activation of the Wnt/β-catenin pathway (45, 46), which plays a key role in the expression of RPE-

specific transcription factors *microphthalmia*-associated transcription factor (MITF) and OTX2 (47). In conjunction with protein paired box 6 (PAX6), MITF and OTX2 are key factors of RPE development (48).

ERG combined with the measurement of ocular retinoid levels revealed the impaired vision of RPE-DKO mice. The significant decrease of retinoids and the histological evidence of retinal degeneration explain the absence of ERG response in these mice. The RPE plays a critical role in providing nutrients to the adjacent retina and in the recycling of the visual chromophore. Upon absorption of light, 11-cis retinal isomerizes to all-trans retinal in the outer segments of the photoreceptors, and the RPE is necessary for the subsequent regeneration of the chromophore throughout the visual cycle (49). The loss of ERK1/2 leads to a decrease in RPE65, and therefore one would expect retinyl ester(s) to accumulate in the RPE cells as reported in RPE65 mutant mice (50). However, in RPE-DKO mice we observed a significant decrease in the retinyl ester(s) both in dark- and light-exposed eyes. Therefore, in addition to RPE65 down-regulation, which could explain the decrease of 11-cis retinal, other pathological alterations in the RPE must account for the decrease in ocular retinoids. We found a mislocalization of LRAT which is mostly expressed at the apical region of the RPE cells in RPE-DKO mice in comparison to its normal basolateral localization (51). This mislocalization could affect LRAT activity and explain the decrease of all-trans retinyl esters. Moreover, we also measured a lower expression of STRA6, an RPE membrane receptor for the retinol binding protein responsible for retinyl ester transport. Because STRA6 and LRAT work together to retrieve retinoids from the blood circulation (52), such diminution may explain the reduction of retinoid content observed in RPE-DKO mice. These results phenocopy some of the phenotypes observed in Stra6$^{-/-}$ mice, including low retinoid content, no ERG response, decrease of BM and RPE lengths, and altered morphology of RPE cells (53).

Alteration of the RPE morphology in RPE-DKO is already visible at 1 month. Whole mounts of RPE from CTL mice show mono- and binucleated hexagonal RPE cells with an apex shared by three cells, while RPE-DKO mice exhibit unusual RPE morphology with a total disappearance of the RPE in some parts of the retina two months after ERK1/2 depletion, whereas other parts display large cells with an irregular shape and multinucleation (Fig. 6). RPE multinucleation, which has been reported in humans (54), could result from a cytokinesis defect . The involvement of cytokinesis defects has been recently described in aging eyes as well as RPE dysfunctions and RPE cell death (55). As ERK1/2 MAP kinase pathway plays a key role in cell proliferation, we could envisage that these kinases might be involved in the process. Sustained activation of ERK1/2 is necessary for the progression from G1 to S phase and is associated with the up-regulation of proliferation-associated genes and the down-regulation of anti-proliferative genes (56). Moreover, ERK1/2 signaling is necessary to allow the entry of RPE cells into cell cycling and RPE cell proliferation (57). In addition to its role in cell cycle control, ERK1/2 are also implicated in the centrosome orientation (58) which is crucial for cytokinesis. Thus we can postulate that disruption of ERK1/2 in RPE induces defects in cell cycle progression, leading to multinucleation of RPE first and then to RPE cell death. Whereas central RPE cells are senescent, the peripheral cells proliferate and ERK1/2 could be important for their maintenance (59, 60). Retinal regeneration in the chick embryo was shown to be dependent on FGF/FGFR/MEK/ERK-dependent upregulation of PAX6 (25). Activation of the ERK1/2 pathway was also responsible for the 15-deoxy-$\Delta^{12,14}$-prostaglandin J_2 ($dPGJ_2$)-dependent protection of RPE cells from oxidative injury (61). These data point not only to a protective role of the ERK1/2 pathway in RPE cells but also to their participation in the maintenance and proliferation of these cells, at least in the peripheral region. Our data indicate that ablation of ERK1/2 in 2 month-old adult RPE cells almost completely abrogated

vision by initiating an early cone-specific degeneration, followed by rod impairment. Surprisingly, we observed a decrease of GNAT1 immunostaining in Cre-DKO mice at 2 and 4 months, which is not observed either by qPCR or Western Blot analysis. At the same time, we clearly detected a decrease in ONL length and thus even if the total GNAT1 retinal content decreases, the TUBULIN abundance decreases in parallel, so that the GNAT1/TUBULIN ratio is not modified. One outstanding question is why are cones more affected than rods in this model? The dependence of cone PR survival on RPE65 has already been reported (62), therefore the direct regulation of RPE65 by ERK1/2 could account, at least in part, for the severe cone dystrophy found in RPE-DKO mice. Moreover, inadequate 11-*cis* retinal production has been shown to be associated with cone degeneration, although the mechanisms are currently not well understood (63-65). The measurement of retinoids specifically in the retina of RPE-DKO mice revealed a significant decrease in 11-*cis*-retinal, which could contribute to the rapid cone degeneration. This finding suggests that the cone-specific effect seen at 2 months could be directly attributed to the ERK1/2 role in regulating RPE65 activity and 11-cis-retinal production that are critical for cone PR survival.

Earlier observations demonstrated that PR degeneration in $Rpe65^{-/-}$ mice caused massive activation of ERK1/2 in the GCL of the retina (23), probably in order to protect the retina against the stress induced by the absence of RPE65. However, we recently showed in polarized ARPE19 cells and isolated mouse RPE that A2E treatment decreases phospho-ERK1/2 significantly along with a reduction of RPE65 level. In addition, inhibition of the ERK1/2 pathway by U0126 also induces a significant decrease of *RPE65* expression (9). The role of ERK1/2 in RPE cells has not been subject to detailed investigation. Our study showing that ERK1/2 loss leads to RPE cell death, retinal atrophy and degeneration strongly supports a significant role for ERK1/2 in the maintenance and survival of RPE cells. Defects of RPE cells

and RPE cells death will lead to PR degeneration. Consistently, these features were observed in a mouse model of genetic RPE ablation that expressed an inducible diphtheria toxin A (DTA) specifically in the RPE. In this RPE^{CreER}/DTA model, functional analysis showed very low scotopic and photopic ERG responses as well as PR degeneration (66). Accordingly, interactions of PR with RPE are essential for PR survival (67).

The very rapid INL degeneration observed in RPE-DKO mice is more difficult to explain. Even if the Cre expression is observed specifically in RPE cells, as shown in the Cre-tdTomato mice (Fig. 1) and as previously described (30), we also noted in certain mice an ectopic expression of Cre in the IPL vessels (but not in the choroidal vessels). Therefore, we cannot totally exclude that ERK1/2 was also depleted in some IPL vessels that may impact on INL degeneration. We can also hypothesize that the absence of key factors normally secreted by the RPE may influence INL degeneration. Further analyses are required in order to decipher the mechanisms leading to INL degeneration in ERK1/2-depleted mice.

Several MEK1/2 inhibitors have been clinically evaluated for cancer therapy but some of these early-phase trials were stopped prematurely because of toxicity issues, including various ocular adverse effects (21, 68-70). Treatments last approximatively 3 weeks and are repeated every month (71, 72). Such long-term treatment with multiple dosing of highly potent MEK inhibitors will lead to a marked and sustained inhibition of ERK1/2 activity, phenocopying in part the impact of the double knockout. We already observed a significant decrease of RPE65 expression at 2 weeks (Fig. 7B) while mRNA and protein levels of this RPE marker are decreased by about 50% at 1 month (Fig. 7C and 7D). Our study provides evidence for a key role of ERK1/2 signaling within the eye and more specifically in RPE cells. Ablation of ERK1/2 signaling reduces *RPE65* expression, leads to decreased retinoid levels, affects RPE and retinal structure, and induces retinal degeneration. Therefore,

the use of ERK1/2 pathway inhibitors in ARMD treatment, as recently suggested (26), has to be re-evaluated taking into consideration the findings reported here. Fine-tuning in ERK1/2 inhibition will be necessary in order to only block the negative effects of high kinase activity and restore low ERK1/2 activity without impacting the role of this kinase in RPE cells.

Materials and methods

Animals

The studies involving mice adhered to the Association for Research in Vision and Ophthalmology (ARVO) statement for the use of animals in ophthalmic and vision research and were approved (permit number VD3023) by the Veterinary service of the State of Vaud (Switzerland). Animals were maintained in 12-h light / 12-h dark cycle with unlimited access to food and water. The generation of *Erk1*$^{-/-}$*/Erk2*$^{fl/fl}$ has been reported previously (29). RPE-specific loss of ERK1/2 (*VMD2-rtTA/TRE-Cre;Erk1*$^{-/-}$*;Erk2*$^{\Delta/\Delta}$ *:* RPE-DKO) was created by cross-breeding the *Erk1*$^{-/-}$*/Erk2*$^{f/f}$ mouse with a mouse expressing the Cre recombinase driven by the human vitelliform macular dystrophy-2 (VMD2) [RPE-Cre] promoter and inducible by doxycycline (30) to first obtain *VMD2-rtTA/TRE-Cre;Erk1*$^{-/-}$*; Erk2*$^{f/f}$. Then two months after birth, VMD2-rtTA/TRE-Cre;Erk1$^{-/-}$;Erk2$^{f/f}$ mice were injected twice, one week apart, with 10ug of doxycycline (Dox) in 500ul PBS in order to induce the Cre recombinase; we call these mice RPE-DKO. As control, Erk1$^{-/-}$/Erk2$^{f/f}$ mice were injected in a similar way with PBS; we call these mice CTL. Every time period mentioned in the experiments refers to the amount of time after Dox injection (e.g. RPE-DKO at 2 months is a 4 month-old mouse treated after 2 months and analyzed 2 months later, after Cre induction and ERK1/2 depletion). Cre-tdTomato mice were created by crossbreeding VMD2-rtTA/TRE-Cre with tdTomato (31) mice to setup the Dox injection protocol and visualize Cre expression. Genotyping of mice was carried out using PCR analysis with genomic DNA isolated from ear punches (Direct PCR

(Ear), Viagen). All the mice were verified for mutant Rd1 negative genotype. The mice were processed for fundus analysis, OCT and ERG or sacrificed for other functional assays at 2w, 1m, 2m, 4m or 1y after the second injection.

Cell culture

HEK293T cells were cultured in high glucose DMEM containing 25 mM of HEPES. The cells were passed every 2-3 days. 600 K cells were seeded in a P60 plate and transfected after 24 hours using calcium-phosphate transfection kit (GE Healthcare) with indicated plasmids, according to the manufacturer's instructions. When indicated cells were treated with 10 nM U0126 (Cell Signaling Technology) or 2 μM PD0325901 (Cell Signaling Technology) for 24 hours and lysed with lysis buffer (20 mM MOPS pH 7.0, 2mM EGTA, 5mM EDTA, 30mM Sodium Fluoride, 60 mM β-Glycerophosphate pH 7.2, 20 mM Sodium Pyrophosphate, 1 mM Sodium Orthovanadate, 1 % Triton-X 100) before analysis.

Non-invasive experiments

Mice were anaesthetized by IP injection of Xylazine 10 mg/kg + Ketamine 80 mg/kg. Mydriatic agents (tropicamide 0.5 %, 2 min; phenylephrine hydrochloride 10 %, 1 min) were applied on the eye for the pupil dilation and to block the eyebrow movement. The fundus of age-matched CTL and RPE-DKO were photographed. OCT was carried out in age-matched CTL and RPE-DKO mice using OCT system (Micron III, Phoenix Research Laboratories) according to the manufacturer's recommendation, at 4 months and 1 year.

For scotopic ERG, age-matched CTL and RPE-DKO mice were dark-adapted overnight before anesthesia and application of the mydriatic agents as described above. For photopic ERG, mice were exposed to bright light of 1000 mAH for 10 minutes. Full-field ERG was recorded using the HMsERG system (Ocuscience).

Immunohistochemistry

Enucleated eyes were fixed in 4% PFA/PBS for 45 min, followed by cryoprotection in 30% sucrose/PBS. 10 µm-embedded frozen sections were further processed for immunohistochemistry. Briefly, frozen retina sections were blocked in PBS with 3% normal goat serum (Sigma-Aldrich) and 0.2% Triton X-100 (Sigma-Aldrich) for 1 h at RT and incubated with primary antibodies in the blocking buffer overnight at 4°C. The following primary antibodies were used: ConeArrestin (Merck Millipore), Rhodopsin (Rho 1D4, a kind gift of Dr. Robert J. Moldy), mOpsin (Chemicon), STRA6 (Abcam), GNAT1 (Santa Cruz Biotechnology), GNAT2 (Santa Cruz Biotechnology), RPE65 (Pin5, a kind gift of Andreas Wenzel), LRAT (Santa Cruz Biotechnology), GFAP (Chemicon), Glycine (ImmunoSolution). Sections were incubated again in blocking buffer for 30 min at RT before incubating with the secondary antibodies for 1 h at RT. Secondary or fluorescent labeled antibodies were: Goat anti-Mouse Alexa Fluor® 488 conjugate, Goat anti-Mouse Alexa Fluor® 594 conjugate, Goat anti-Rabbit Alexa Fluor® 488 conjugate, Goat anti-Rabbit Alexa Fluor® 594 conjugate, Oregon Green® 488 Phalloidin (Thermo Fisher Scientific). Incubation with secondary antibody alone was used as a negative control. Tissue sections were counterstained with DAPI to identify retinal cell layers.

For flatmount choroid-RPE structure, dissected choroid-RPE sections were mounted on a cover slip, fixed in 4% PFA/PBS for 45 min and processed for immune labeling with Oregon as described. TUNEL assay (Roche Life Science) was carried out as already described (23).

Tissue isolation, mRNA extraction and protein preparation

Enucleated eyes from CTL and RPE-DKO were dissected under a microscope to exclude extra-ocular tissues. The cornea, lens, iris, and vitreous body were removed and the retina extracted. Either the retina, the RPE or the RPE-choroid were processed for protein/mRNA isolation.

For mRNA extraction, either the retina or the RPE-choroid were resuspended in TRIzol (TRIzol® Reagent, ThermoFisher) and stored at -80 °C until further handling. RPE mRNA was extracted using a previously described protocol (73), while retinas and RPE-choroids were extracted using the following protocol. Briefly, 0.1 volume of sodium acetate, 1 volume of phenol and 0.2 volume of chloroform were added to the tube, mixed and phase separation was allowed on ice for 15 minutes. 1 volume of isopropanol and 2 µl of glycogen (5 µg/µl) were added to the upper aqueous phase and left to precipitate at -20^{0}C overnight. Following centrifugation at 10,000g for 10 min at 4^{0}C, the precipitate was washed with 75 % EtOH, and allowed to dry at RT before being resuspended in ddH2O DEPC. Quantitative PCR was carried out as already described (23) using 100 nM primers. The sets of primers used for genotyping (Fig. 1B) and RT-PCR can be found in table 1.

Protein isolation from retinas was performed by two successive homogenizations of the retina with syringes (23G and 26G) on ice, followed by 3 freeze/thaw cycles. RPE cell lysates were prepared as previously described (74). Briefly, incised RPE/Choroid was incubated in RIPA (50mM Tris pH8.0, 150mM NaCl, 1% NP-40, 0.5% sodium deoxycholate, 0.1% SDS) buffer for 10 min with shaking. The choroid was transferred to a different tube leaving the shredded RPE cells on the tube wall.

For western blot analysis, extracted retinas were resuspended in lysis buffer (20mM MOPS pH7.0, 2mM EGTA, 5mM EDTA, 30 mM sodium fluoride, 60 mM-B-gylcerophosphate pH7.2, 20mM sodium pyrophosphate, 1mM sodium orthovanadate, 1% TritonX-100, DTT 1M + protease inhibitors) while RPE were resuspended in RIPA buffer (50mM Tris pH8.0, 150mM NaCl, 1% NP-40, 0.5% sodium deoxycholate, 0.1% SDS). All samples were conserved at -80 ^{0}C until further processed. Extracted cell lysates were separated by SDS–PAGE and transferred onto nitrocellulose membranes (Millipore). The membranes were probed using the indicated primary antibodies and isotype-matched secondary antibodies conjugated

to fluorescence (Licor Biosciences) and detected using the Odyssey imaging system (Licor). The following primary antibodies were utilized: GNAT 1 (Santa Cruz Biotechnology), GNAT2 (Santa Cruz Biotechnology), ERK1/2 (Cell Signaling Technology), α-TUBULIN (Sigma-Aldrich), RPE65 (Pin5). Following secondary bodies were applied: IRDye 680RD (LI-COR Biosciences), IRDye 800CW (LI-COR Biosciences).

Luciferase and AP-1 binding assays

Luciferase activity was measured in cell lysates using a coenzyme A-coupled assay system containing luciferin and ATP (Promega). Ten µg of cell lysates were mixed with 20 µl of luciferase assay reagent in 4 triplicates. Lum/E was read using a kinetic software on a 384 well plate spectrophotometer (PerkinElmer). Beta-galactosidase activity was measured using a luminescent substrate endpoint assay. 20 µg of lysates were mixed with 50 µl β-gal buffer 2x (Na_2HPO_4 120 mM, NaH_2PO_4 80 mM, $MgCl_2$ 2 mM and β-ME 100 mM) and 50 µl ONPG 2x (2-Nitrophenyl-B-D-Galactopyranoside). The absorbance at 412 nm was read.

AP-1 binding assay (TransAM AP-1 kit, Active Motif) was carried out as described (24) on nuclear extracts from ARPE19 cells. Briefly, cells were resuspended in 1 ml cold buffer A (10 mM Hepes, pH 7.9, 10 mM KCl, 1 mM DTT and protease inhibitors) and placed for 15 min on ice. Then 12.5 µl of 10% NP-40 was added and the supernatant was discarded after centrifugation. Nuclei were lysed in buffer B (20 mM Hepes, pH 7.9, 400 mM NaCl, 1 mM DTT and protease inhibitors) and quantified for protein content. 8 µg of nuclear protein extract or 15 µg of whole cell protein extracts were used for AP-1 binding assay as described by the manufacturer.

AP-1 EMSA Assay

AP-1 EMSA assay was carried out on nuclear extracts from HEK293 cells either left untreated or treated with U0126 following the protocol of the provider (Odyssey®

559 Infrared EMSA Kit, LI-COR Biosciences). In brief, the nuclear extract was incubated
560 with 25 mM DTT/2.5% Tween-20, 1 µg/µl Ploy (dI.dC), 1% NP-40, 100 mM MgCl2,
561 IRDye 700 AP-1 Consensus Oligo (5'-CGCTTG A*TG ACT CA*G CCG GAA-3') either
562 in the presence or absence of AP-1 competitor oligo. The binding was performed for
563 20 minutes after which the sample was loaded on a 5% Native Acrylamid gel in the
564 presence of a loading dye. The fluorescence was detected on LI-COR Odyssey
565 scanner.
566 *Retinoid measurement*
567 Age-matched CTL and RPE-DKO mice were either dark-adapted overnight or
568 exposed to bright light of 1000 mAH for 2 hours. For the dark condition, the retina
569 was separated from the RPE-choroid layer. For the bright light condition, the whole
570 eye was processed for the measurement. Ocular tissues were transferred into a 2 ml
571 reaction vial and 200 µl of 2 M hydroxylamine (pH 6.8) and 200 µl of methanol were
572 added. All steps were conducted under red safety light (> 600 nm) to avoid retinoid
573 isomerization. Tissues were mechanically grinded using a Bio-Gen PRO200
574 homogenizer (Fisher Scientific). The homogenized extracts were allowed to stand for
575 10 min for oxime formation. Then, 400 µl of acetone and 500 µl of hexane were
576 added. The samples were vortexed and the aqueous and organic phases were
577 separated by centrifugation at 5,000 x g (Eppendorf Minispin plus). The organic
578 phase was removed and the extraction was repeated with 500 µl of hexane.
579 Collected organic phases were pooled and dried with a SpeedVac (Eppendorf) at
580 30^{o}C and re-dissolved in HPLC mobile phase solvent. The HPLC analysis was
581 carried out with an Agilent 1260 Infinity Quaternary HPLC system (Santa Clara)
582 equipped with a pump (G1312C) with an integrated degasser (G1322A), a
583 thermostated column compartment (G1316A), an autosampler (G1329B), a diode-
584 array detector (G1315D), and online analysis software (Chemstation). The analyses
585 were carried out at 25^{o}C using a normal-phase Zorbax Sil (5 µm, 4.6 x 150 mm)

column (Agilent Technologies) protected with a guard column with the same stationary phase. For retinoid separation, the column was developed with 90% hexane and 10% ethyl acetate with an isocratic flow rate of 1.4 ml x min^{-1}. For molar quantification of retinoids the HPLC system was scaled with authentic retinoid standards.

Electron Microscopy

Enucleated whole mouse eyes were fixed in glutaraldehyde solution (Electron Microscopy Sciences) 2.5% in Phosphate Buffer (PB 0.1M pH7.4) (Sigma-Aldrich) for 90 min at room temperature (RT). Then, ocular tissues were post-fixed by a fresh mixture of osmium tetroxide 1% (Electron Microscopy Sciences) with 1.5% of potassium ferrocyanide (Sigma-Aldrich) in PB buffer during 1h30 at RT. The samples were then washed three times in distilled water and dehydrated in graded concentrations of acetone solution (Sigma-Aldrich) (30%-20min; 70%-20min; 100%-1h; 100%-2h). This was followed by infiltration in graded concentrations of Epon (Sigma-Aldrich) (2h Epon-acetone: 1/3; 2h Epon-acetone: 3/1; 4h and 12h Epon-acetone: 1/1) and finally polymerized for 48h at 60°C in an oven. Ultrathin sections of 50nm were cut transversally on a Leica Ultracut (Leica Microsystems) and picked up on a nickel slot grid 2x1mm (Electron Microscopy Sciences) coated with a polystyrene film (Sigma-Aldrich). Sections were post-stained with uranyl acetate (Sigma-Aldrich) 4% in H_2O during 10 minutes, rinsed several times with H_2O followed by Reynold's (Reynolds ES. 1963. J Cell Biol, 17, 208-212) lead citrate 0.4% in H_2O (Sigma-Aldrich) during 10 minutes and rinsed several times with H_2O.

Micrographs were taken with a transmission electron microscope Philips CM100 (now FEI Company) at an acceleration voltage of 80kV with a TVIPS TemCam-F416 digital camera (TVIPS GmbH).

Molecular biology

pGL2-Basic-RPE65 (-450/+39) was a kind gift of Dr. Debra Thompson (University of Michigan). pGL3-Basic-LRAT (-268/+257) was a kind gift of Dr. Catharine Ross (University of Pennsylvania). pGL2-Basic-RPE65 (-450/+39) (33) was digested by BglII and StuI and re-ligated in order to remove the (190 bp segment from the start codon) AP-1 site.

References

1. **Hageman GS, Luthert PJ, Chong NHV, Johnson LV, Anderson DH, Mullins RF.** 2001. An integrated hypothesis that considers drusen as biomarkers of immune-mediated processes at the RPE-Bruch's membrane interface in aging and age-related macular degeneration. Prog Retin Eye Res **20:**705-732.

2. **Rodrigues EB.** 2007. Inflammation in dry age-related macular degeneration. Ophthalmologica **221:**143-152.

3. **Zhou JL, Jang YP, Kim SR, Sparrow JR.** 2006. Complement activation by photooxidation products of A2E, a lipofuscin constituent of the retinal pigment epithelium. Proc Natl Acad Sci USA **103:**16182-16187.

4. **Iriyama A, Fujiki R, Inoue Y, Takahashi H, Tamaki Y, Takezawa S, Takeyama K, Jang WD, Kato S, Yanagi Y.** 2008. A2E, a pigment of the lipofuscin of retinal pigment epithelial cells, is an endogenous ligand for retinoic acid receptor. J Biol Chem **283:**11947-11953.

5. **Eldred GE, Lasky MR.** 1993. Retinal Age Pigments Generated by Self-Assembling Lysosomotropic Detergents. Nature **361:**724-726.

6. **Ablonczy Z, Higbee D, Anderson DM, Dahrouj M, Grey AC, Gutierrez D, Koutalos Y, Schey KL, Hanneken A, Crouch RK.** 2013. Lack of Correlation Between the Spatial Distribution of A2E and Lipofuscin Fluorescence in the Human Retinal Pigment Epithelium. Invest Ophthalmol Vis Sci **54:**5535-5542.

7. **Sparrow JR, Boulton M.** 2005. RPE lipofuscin and its role in retinal-pathobiology. Exp Eye Res **80:**595-606.

8. **Holz FG, Schutt F, Kopitz J, Eldred GE, Kruse FE, Volcker HE, Cantz M.** 1999. Inhibition of lysosomal degradative functions in RPE cells by a retinoid component of lipofuscin. Invest Ophthalmol Vis Sci **40:**737-743.

9. **Balmer D, Bapst-Wicht L, Pyakurel A, Emery M, Nanchen N, Bochet CG, Roduit R.** 2017. Bis-retinoid A2E Induces an Increase of basic Fibroblast Growth Factor via Inhibition of Extracellular signal-Regulated Kinases 1/2 Pathway in Retinal Pigment Epithelium Cells and Facilitates Phagocytosis. Frontiers Aging Neuroscience **9:**43.

10. **Cargnello M, Roux PP.** 2011. Activation and function of the MAPKs and their substrates, the MAPK-activated protein kinases. Microbiology and molecular biology reviews : MMBR **75:**50-83.

11. **Plotnikov A, Zehorai E, Procaccia S, Seger R.** 2011. The MAPK cascades: signaling components, nuclear roles and mechanisms of nuclear translocation. Biochimica et Biophysica Acta **1813**.

12. **Kyriakis JM, Avruch J.** 2012. Mammalian MAPK signal transduction pathways activated by stress and inflammation: a 10-year update. Physiological Reviews **92:**689-737.

13. **Davis RJ.** 1995. Transcriptional regulation by MAP kinases. Molecular Reproduction and Development **42:**459-467.

14. **Lawrence MC, Jivan A, Shao C, Duan L, Goad D, Zaganjor E, Osborne J, McGlynn K, Stippec S, Earnest S, Chen W, Cobb MH.** 2008. The roles of MAPKs in disease. Cell Res **18:**436-442.

15. **Schubbert S, Shannon K, Bollag G.** 2007. Hyperactive Ras in developmental disorders and cancer. Nature Reviews Cancer **7:**295-308.

16. **Kim EK, Choi E-JJ.** 2010. Pathological roles of MAPK signaling pathways in human diseases. Biochimica et Biophysica Acta **1802:**396-405.

17. **Rauen KA.** 2013. The RASopathies. Annual Review of Genomics and Human Genetics **14:**355-369.

18. **Fremin C, Meloche S.** 2010. From basic research to clinical development of MEK1/2 inhibitors for cancer therapy. J Hematol Oncol **3:**8.

19. **Samatar AA, Poulikakos PI.** 2014. Targeting RAS-ERK signalling in cancer: promises and challenges. Nature Reviews Drug discovery **13:**928-942.

20. **Martinez-Garcia M, Banerji U, Albanell J, Bahleda R, Dolly S, Kraeber-Bodere F, Rojo F, Routier E, Guarin E, Xu ZX, Rueger R, Tessier JJL, Shochat E, Blotner S, Naegelen VM, Soria JC.** 2012. First-in-Human, Phase I Dose-Escalation Study of the Safety, Pharmacokinetics, and Pharmacodynamics of RO5126766, a First-in-Class Dual MEK/RAF Inhibitor in Patients with Solid Tumors. Clin Cancer Res **18:**4806-4819.

21. **Duncan KE, Chang LY, Patronas M.** 2015. MEK inhibitors: a new class of chemotherapeutic agents with ocular toxicity. Eye **29:**1003-1012.

22. **Donovan M, Doonan F, Cotter TG.** 2011. Differential roles of ERK1/2 and JNK in retinal development and degeneration. J Neurochem **116:**33-42.

23. **Metrailler S, Emery M, Schorderet DF, Cottet S, Roduit R.** 2013. ERK1/2 pathway is activated in degenerated Rpe65-deficient mice. Exp Eye Res **116:**86-95.

24. **Roduit R, Schorderet DF.** 2008. MAP kinase pathways in UV-induced apoptosis of retinal pigment epithelium ARPE19 cells. Apoptosis **13:**343-353.

25. **Spence JR, Madhavan M, Aycinena JC, Del Rio-Tsonis K.** 2007. Retina regeneration in the chick embryo is not induced by spontaneous Mitf downregulation but requires FGF/FGFR/MEK/Erk dependent upregulation of Pax6. Mol Vis **13:**57-65.

26. **Dridi S, Hirano Y, Tarallo V, Kim Y, Fowler BJ, Ambati BK, Bogdanovich S, Chiodo VA, Hauswirth WW, Kugel JF, Goodrich JA, Ponicsan SL, Hinton DR, Kleinman ME, Baffi JZ, Gelfand BD, Ambati J.** 2012. ERK1/2 activation is a

691 therapeutic target in age-related macular degeneration. Proc Natl Acad Sci USA
692 **109:**13781-13786.
693 27. **Subramaniam S, Unsicker K.** 2010. ERK and cell death: ERK1/2 in neuronal
694 death. Febs J **277:**22-29.
695 28. **Pyakurel A, Savoia C, Hess D, Scorrano L.** 2015. Extracellular Regulated
696 Kinase Phosphorylates Mitofusin 1 to Control Mitochondrial Morphology and
697 Apoptosis. Mol Cell **58:**244-254.
698 29. **Voisin L, Saba-El-Leil MK, Julien C, Fremin C, Meloche S.** 2010. Genetic
699 demonstration of a redundant role of extracellular signal-regulated kinase 1 (ERK1)
700 and ERK2 mitogen-activated protein kinases in promoting fibroblast proliferation. Mol
701 Cell Biol **30:**2918-2932.
702 30. **Le YZ, Zheng W, Rao PC, Zheng LX, Anderson RE, Esumi N, Zack DJ,**
703 **Zhu ML.** 2008. Inducible expression of Cre recombinase in the retinal Pigmented
704 epithelium. Invest Ophthalmol Vis Sci **49:**1248-1253.
705 31. **Madisen L, Zwingman TA, Sunkin SM, Oh SW, Zariwala HA, Gu H, Ng LL,**
706 **Palmiter RD, Hawrylycz MJ, Jones AR, Lein ES, Zeng HK.** 2010. A robust and
707 high-throughput Cre reporting and characterization system for the whole mouse
708 brain. Nat Neurosci **13:**133-U311.
709 32. **Lampert JM, Holzschuh J, Hessel S, Driever W, Vogt K, von Lintig J.**
710 2003. Provitamin A conversion to retinal via the beta,beta-carotene-15,15'-oxygenase
711 (bcox) is essential for pattern formation and differentiation during zebrafish
712 embryogenesis. Development **130:**2173-2186.
713 33. **Nicoletti A, Kawase K, Thompson DA.** 1998. Promoter analysis of RPE65,
714 the gene encoding a 61-kDa retinal pigment epithelium-specific protein. Invest
715 Ophthalmol Vis Sci **39:**637-644.

34. **Zolfaghari R, Ross AC.** 2009. An essential set of basic DNA response elements is required for receptor-dependent transcription of the lecithin:retinol acyltransferase (Lrat) gene. Archives of Biochemistry and Biophysics **489:**1-9.

35. **Redmond TM, Yu S, Lee E, Bok D, Hamasaki D, Chen N, Goletz P, Ma JX, Crouch RK, Pfeifer K.** 1998. Rpe65 is necessary for production of 11-cis-vitamin A in the retinal visual cycle. Nat Genet **20:**344-351.

36. **Morimura H, Fishman GA, Grover SA, Fulton AB, Berson EL, Dryja TP.** 1998. Mutations in the RPE65 gene in patients with autosomal recessive retinitis pigmentosa or leber congenital amaurosis. Proc Natl Acad Sci USA **95:**3088-3093.

37. **Lorenz B, Gyurus P, Preising M, Bremser D, Gu SM, Andrassi M, Gerth C, Gal A.** 2000. Early-onset severe rod-cone dystrophy in young children with RPE65 mutations. Invest Ophthalmol Vis Sci **41:**2735-2742.

38. **Redmond TM, Poliakov E, Yu S, Tsai JY, Lu ZJ, Gentleman S.** 2005. Mutation of key residues of RPE65 abolishes its enzymatic role as isomerohydrolase in the visual cycle. Proc Natl Acad Sci USA **102:**13658-13663.

39. **Boulanger A, Liu SY, Henningsgaard AA, Yu S, Redmond TM.** 2000. The upstream region of the Rpe65 gene confers retinal pigment epithelium-specific expression in vivo and in vitro and contains critical octamer and E-box binding sites. J Biol Chem **275:**31274-31282.

40. **Chen Y, Ma JX, Crouch RK.** 2003. Down-regulation of RPE65 protein expression and promoter activity by retinoic acid. Mol Vis **9:**345-354.

41. **Li SH, Lee J, Zhou YD, Gordon WC, Hill JM, Bazan NG, Miner JH, Jin MH.** 2013. Fatty Acid Transport Protein 4 (FATP4) Prevents Light-Induced Degeneration of Cone and Rod Photoreceptors by Inhibiting RPE65 Isomerase. J Neurosci **33:**3178-3189.

42. **Masuda T, Wahlin K, Wan J, Hu JF, Maruotti J, Yang X, Iacovelli J, Wolkow N, Kist R, Dunaief JL, Qian J, Zack DJ, Esumi N.** 2014. Transcription

743 Factor SOX9 Plays a Key Role in the Regulation of Visual Cycle Gene Expression in
744 the Retinal Pigment Epithelium. J Biol Chem **289:**12908-12921.
745 43. **Ling SZ, Chang XF, Schultz L, Lee TK, Chaux A, Marchionni L, Netto GJ,**
746 **Sidransky D, Berman DM.** 2011. An EGFR-ERK-SOX9 Signaling Cascade Links
747 Urothelial Development and Regeneration to Cancer. Cancer Res **71:**3812-3821.
748 44. **Sun D, Zhang Y, Wang C, Hua X, Zhang XA, Yan J.** 2013. Sox9-related
749 signaling controls zebrafish juvenile ovary-testis transformation. Cell Death Dis **4**.
750 45. **Cervenka I, Wolf J, Masšek J, Krejci P, Wilcox WR, Kozubík A, Schulte G,**
751 **Gutkind SJ, Bryja V.** 2011. Mitogen-activated protein kinases promote WNT/ -
752 catenin signaling via phosphorylation of LRP6. Molecular and Cellular Biology
753 **31:**179-189.
754 46. **Lemieux E, Cagnol S, Beaudry K, Carrier J, Rivard N.** 2015. Oncogenic
755 KRAS signalling promotes the Wnt/β-catenin pathway through LRP6 in colorectal
756 cancer. Oncogene **34:**4914– 4927.
757 47. **Westenskow P, Piccolo S, Fuhrmann S.** 2009. Beta-catenin controls
758 differentiation of the retinal pigment epithelium in the mouse optic cup by regulating
759 Mitf and Otx2 expression. Development **136:**2505-2510.
760 48. **Bharti K, Gasper M, Ou J, Brucato M.** 2012. A regulatory loop involving
761 PAX6, MITF, and WNT signaling controls retinal pigment epithelium development.
762 PLoS Genet **8**.
763 49. **Rando RR.** 2001. The biochemistry of the visual cycle. Chem Rev **101:**1881-
764 1896.
765 50. **Katz ML, Redmond TM.** 2001. Effect of Rpe65 knockout on accumulation of
766 lipofuscin fluorophores in the retinal pigment epithelium. Invest Ophthalmol Vis Sci
767 **42:**3023-3030.
768 51. **Huang J, Possin DE, Saari JC.** 2009. Localizations of visual cycle
769 components in retinal pigment epithelium. Mol Vis **15:**223-234.

52. **Amengual J, Golczak M, Palczewski K, von Lintig J.** 2012. Lecithin: Retinol Acyltransferase Is Critical for Cellular Uptake of Vitamin A from Serum Retinol-binding Protein. J Biol Chem **287:**24216-24227.

53. **Amengual J, Zhang N, Kemerer M, Maeda T, Palczewski K, Von Lintig J.** 2014. STRA6 is critical for cellular vitamin A uptake and homeostasis. Hum Mol Genet **23:**5402-5417.

54. **Starnes AC, Huisingh C, McGwin G, Jr., Sloan KR, Ablonczy Z, Smith RT, Curcio CA, Ach T.** 2016. Multi-nucleate retinal pigment epithelium cells of the human macula exhibit a characteristic and highly specific distribution. Vis Neurosci **33:**e001.

55. **Chen M, Rajapakse D, Fraczek M, Luo C, Forrester JV, Xu H.** 2016. Retinal pigment epithelial cell multinucleation in the aging eye - a mechanism to repair damage and maintain homoeostasis. Aging Cell **15:**436-445.

56. **Meloche S, Pouyssegur J.** 2007. The ERK1/2 mitogen-activated protein kinase pathway as a master regulator of the G1- to S-phase transition. Oncogene **26:**3227-3239.

57. **Yoshikawa T, Mizuno A, Yasumuro H.** 2012. MEK‐ERK and heparin - susceptible signaling pathways are involved in cell - cycle entry of the wound edge retinal pigment epithelium cells in the adult newt. Pigment Cell Melanoma Res **25:**66-82.

58. **Bisel B, Wang YZ, Wei JH, Xiang Y, Tang DM, Miron-Mendoza M, Yoshimura S, Nakamura N, Seemann J.** 2008. ERK regulates Golgi and centrosome orientation towards the leading edge through GRASP65. J Cell Biol **182:**837-843.

59. **Kokkinopoulos I, Shahabi G, Colman A, Jeffery G.** 2011. Mature Peripheral RPE Cells Have an Intrinsic Capacity to Proliferate; A Potential Regulatory Mechanism for Age-Related Cell Loss. Plos One **6**.

60. **Hecquet C, Lefevre G, Valtink M, Engelmann K, Mascarelli F.** 2002. Activation and role of MAP kinase-dependent pathways in retinal pigment epithelial cells: ERK and RPE cell proliferation. Invest Ophthalmol Vis Sci **43:**3091-3098.

61. **Qin S, McLaughlin AP, De Vries GW.** 2006. Protection of RPE cells from oxidative injury by 15-deoxy-delta12,14-prostaglandin J2 by augmenting GSH and activating MAPK. Invest Ophthalmol Vis Sci **47:**5098-5105.

62. **Wenzel A, von Lintig J, Oberhauser V, Tanimoto N, Grimm C, Seeliger MW.** 2007. RPE65 is essential for the function of cone photoreceptors in NRL-deficient mice. Invest Ophthalmol Vis Sci **48:**534-542.

63. **Rohrer B, Lohr HR, Humphries P, Redmond TM, Seeliger MW, Crouch RK.** 2005. Cone opsin mislocalization in Rpe65-/- mice: a defect that can be corrected by 11-cis retinal. Invest Ophthalmol Vis Sci **46:**3876-3882.

64. **Tang PH, Fan J, Goletz PW, Wheless L, Crouch RK.** 2010. Effective and Sustained Delivery of Hydrophobic Retinoids to Photoreceptors. Invest Ophthalmol Vis Sci **51:**5958-5964.

65. **Znoiko SL, Rohrer B, Lu KN, Lohr HR, Crouch RK, Ma JX.** 2005. Downregulation of cone-specific gene expression and degeneration of cone Photoreceptors in the Rpe65(-/-) mouse at early ages. Invest Ophthalmol Vis Sci **46:**1473-1479.

66. **Longbottom R, Fruttiger M, Douglas RH, Martinez-Barbera JP, Greenwood J, Moss SE.** 2009. Genetic ablation of retinal pigment epithelial cells reveals the adaptive response of the epithelium and impact on photoreceptors. Proc Natl Acad Sci USA **106:**18728-18733.

820 67. **Strauss O.** 2005. The retinal pigment epithelium in visual function. Physiol
821 Rev **85:**845-881.
822 68. **Renouf DJ, Velazquez-Martin JP, Simpson R, Siu LL, Bedard PL.** 2012.
823 Ocular Toxicity of Targeted Therapies. J Clin Oncol **30:**3277-3286.
824 69. **Niro A, Strippoli S, Alessio G, Sborgia L, Recchimurzo N, Guida M.** 2015.
825 Ocular Toxicity in Metastatic Melanoma Patients Treated With Mitogen-Activated
826 Protein Kinase Kinase Inhibitors: A Case Series. Am J Ophthalmol **160:**959-967.
827 70. **Schoenberger SD, Kim SJ.** 2013. Bilateral Multifocal Central Serous-Like
828 Chorioretinopathy due to MEK Inhibition for Metastatic Cutaneous Melanoma. Case
829 Reports in Ophthalmol Med **2013:**673796.
830 71. **Haura EB, Ricart AD, Larson TG, Stella PJ, Bazhenova L, Miller VA,**
831 **Cohen RB, Eisenberg PD, Selaru P, Wilner KD, Gadgeel SM.** 2010. A phase II
832 study of PD-0325901, an oral MEK inhibitor, in previously treated patients with
833 advanced non-small cell lung cancer. Clinical Cancer Research : an official journal of
834 the American Association for Cancer Research **16:**2450-2457.
835 72. **Rinehart J, Adjei AA, LoRusso PM.** 2004. Multicenter phase II study of the
836 oral MEK inhibitor, CI-1040, in patients with advanced non-small-cell lung, breast,
837 colon, and pancreatic cancer. J Clin Oncol **22:**4456-4462.
838 73. **Xin-Zhao Wang C, Zhang K, Aredo B, Lu H, Ufret-Vincenty RL.** 2012.
839 Novel method for the rapid isolation of RPE cells specifically for RNA extraction and
840 analysis. Exp Eye Res **102:**1-9.
841 74. **Wei H, Xun Z, Granado H, Wu A, Handa JT.** 2015. An easy, rapid method to
842 isolate RPE cell protein from the mouse eye. Exp Eye Res **145:**450-455.

843 **Figure Legends**

844 **Fig. 1: Generation and characterization of CTL and RPE-DKO mice.** (A)
845 tdTomato fluorescence of the cryostat section of a fixed whole mount eye from

Cre/tdTomato mice injected with either PBS or doxycycline (Dox). (B) Constructs used to generate the Erk1-KO and Erk2 conditional mice ($Erk1^{-/-}Erk2^{f/f}$) and primers used to genotype the mice. (C) Representative genotyping of $Erk1^{+/-};Erk2^{+/f}$ (lane 1), $Erk1^{-/-};Erk2^{f/f}$ called CTL (lane 2) and VMD2-rtTA/TRE-Cre;$Erk1^{-/-};Erk2^{lx/lx}$ called RPE-DKO, when injected with Dox (lane 3). (D) The specific loss of Erk2 in RPE is confirmed by the delta fragment present in genomic DNA isolated from RPE cells; $Erk1^{+/-};Erk2^{+/f}$ (lane 1), $Erk1^{-/-};Erk2^{f/f}$ called CTL (lane 2) and VMD2-rtTA/TRE-Cre;$Erk1^{-/-};Erk2^{lx/lx}$ called RPE-DKO, when injected with Dox (lane 3). (E) Cryostat section of fixed whole mount eyes, from CTL and RPE-DKO at 1 month, immunostained as indicated. (F) Western blot analysis of ERK1/2 expression in RPE protein lysates from CTL and RPE-DKO at 1 month; ARPE19 protein lysate is used as positive control for ERK1 expression.

Fig. 2: Loss of ERK1/2 in RPE leads to vision impairment. (A) Representative fundus images of CTL and RPE-DKO at 2 or 4 months. (B) Representative OCT images of CTL and RPE-DKO at 4 months. (C) Graphs of the scotopic (n=10) and photopic (n=4) ERG responses (b wave) taken in CTL and RPE-DKO at 2 months. (*$p<0.05$, **$p<0.001$). The right panel shows the scotopic (50 mcd s/m2) and the photopic (10 mcd s/m2) ERG response of CTL and RPE-DKO mice. (D) Chromatographs and quantification of retinoids measured in the retina and in the RPE/choroid from mice at 1 month, dark-adapted for 16 hours or measured in whole eye (containing retina, RPE and choroid) from mice (same conditions) exposed to 1000 mA of light for 2 hours.

Fig. 3: Loss of ERK1/2 in RPE leads to photoreceptor degeneration. (A) Cryostat section of fixed whole mount eye, from CTL and RPE-DKO at 2 or 4 months, immunostained against different rod and cone markers as indicated. (B) Flatmount retinal preparation, from CTL and RPE-DKO at 4 months, immunostained as indicated. (C) Outer nuclear layer (ONL) and inner nuclear layer (INL) lengths

measured manually using ImageJ. Data represent mean ± SEM of four independent experiments *p<0.05. (D) GNAT1 and ConeArrestin stainings from CTL and RPE-DKO at 1 month. Presence of both photoreceptor markers was observed in the RPE of RPE-DKO mice (white arrows). (E) TUNEL staining of cryostat section of fixed whole mount eye from CTL and RPE-DKO at 2 months.

Fig. 4: Outer nuclear layer (ONL), outer segment (OS) and inner segment (IS) decrease from the start of degeneration to complete absence in RPE-DKO at 1 year. (A) Electron microscopy images of retina-RPE layers from CTL and RPE-DKO at 2 or 4 months. The bottom panel is a magnification of outer segment (OS) layer of photoreceptors (PR). (B) Measurement of outer nuclear layer (ONL), outer segment (OS) and inner segment (IS) from electron microscopy images. Data represent mean ± SEM of 3 experiments, **p<0.008. (C) Cryostat section of fixed whole mount eye, from CTL and RPE-DKO at 1 year, immunostained as indicated.

Fig. 5: Loss of ERK1/2 in RPE causes specific reduction in cone markers. (A) Representative images and quantification graphs of retinal protein lysates from CTL and RPE-DKO at 1, 2 or 4 months. Data represent mean ± SEM of 5 independent experiments (*p<0.02, **p<0.001). (B) Quantification graphs of QPCR performed on retinal extracts from CTL and RPE-DKO at 1, 2 or 4 months. RL8 was used as internal control to normalize RNA expression. Results are expressed as percentage of CTL and as mean ± SEM of 4 independent experiments (*p<0.05, **p<0.003).

Fig. 6: Loss of ERK1/2 in RPE leads to massive ultrastructural changes in RPE-DKO at 1 month. (A) Representative electron microscopy images showing different retinal and RPE cell layers (B, Bruch's Membrane; RPE, Retinal Pigment Epithelium; OS, Outer Segment; IS, Inner Segment; ONL, Outer Nuclear Layer). (B) Representative electron microscopy image of the Bruch's membrane (B, Bruch's membrane) and the underlying RPE cells and measurement of Bruch's membrane length (*p<0.0001). (C) Representative electron microscopy image of the RPE cell

layer and the underlying OS of the PR, and measurement of RPE length and quantification of the area of mitochondria (stars: mitochondria) (*p<0.015). (D) Electron microscopy image showing the accumulation of membrane-enriched phagolysosomes in the RPE of RPE-DKO in comparison to CTL (white arrows). (E and F) RPE flatmount from CTL and RPE-DKO at 2 months, immunostained against Phalloidin and counterstained with Dapi.

Fig. 7: ERK1/2 directly regulates RPE65 expression. (A) Cryostat section of fixed whole mount eyes, from CTL and RPE-DKO at 1 month, immunostained as indicated. (B) Cryostat section of fixed whole mount eyes, from CTL and RPE-DKO at 2 weeks, immunostained as indicated. (C) QPCR analysis of mRNA extracted from the RPE/choroid of CTL and RPE-DKO at 1 month, for the genes indicated. RL8 was used as internal control to normalize RNA expression. Results are expressed as percentage of CTL and as mean ± SEM of 3 retinas, *p<0.03. (D) Representative immunoblot and quantification of RPE protein lysates from CTL and RPE-DKO at 1 month, immunoblotted as indicated, **p<0.0002, n=5. (E) Luciferase assay for both RPE65 and LRAT promoters. HEK293 cells were transfected and treated as indicated. The luciferase fluorescence was normalized to β-gal fluorescence. Data represent mean ± SEM of 4 independent experiments, *p<0.05 vs pGL2-Basic-RPE65, #p<0.05 vs pGL2-Basic. (F) EMSA assay of AP-1 complex in nucleus from ARPE19 cells treated or not with U0126. AP-1 DNA binding analysis from nuclear extract of ARPE19 cells treated either with U0126 or PD0325901. Data represent mean ± SEM of 3 independent experiments expressed as percentage of control, *p<0.02, **p<0.002. (G) AP-1 DNA binding analysis of whole cell extracts from mice at 1 month. Data represent mean ± SEM of 3 independent experiments expressed as percentage of control, *p<0.015, **p<0.002, n=6. Representative immunoblot of RPE protein lysates from CTL and RPE-DKO at 1 month, showing the expression of C-FOS and FRA-1; TUBULIN was used as control.

927 **Table 1: Primers used for genotyping and qPCR**

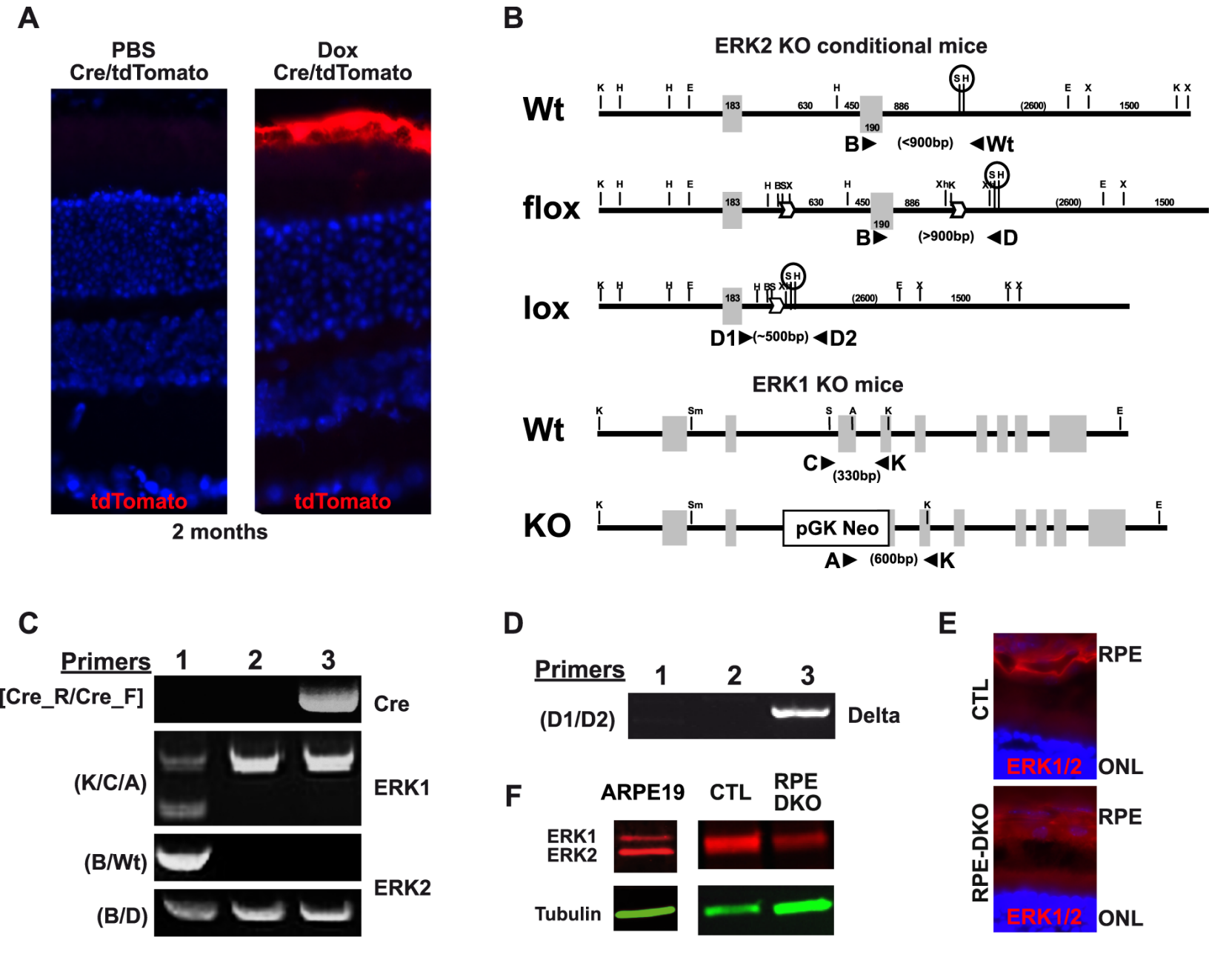

Fig. 1: Generation and characterization of CTL and RPE-DKO mice. (A) tdTomato fluorescence of the cryostat section of fixed whole mount eye from Cre/tdTomato mice injected with either PBS or doxycycline (Dox). (B) Constructs used to generate the Erk1-KO and Erk2 conditional mice ($Erk1^{-/-}$ $Erk2^{f/f}$) and primers used to genotype the mice. (C) Representative genotyping of $Erk1^{+/-}$;$Erk2^{+/f}$ (lane 1), $Erk1^{-/-}$;$Erk2^{f/f}$ called CTL (lane 2) and VMD2-rtTA/TRE-Cre;$Erk1^{-/-}$;$Erk2^{lx/lx}$ called RPE-DKO, when injected with Dox (lane 3). (D) The specific loss of Erk2 in RPE is confirmed by the delta fragment present in genomic DNA isolated from RPE cells; $Erk1^{+/-}$;$Erk2^{+/f}$ (lane 1), $Erk1^{-/-}$;$Erk2^{f/f}$ called CTL (lane 2) and VMD2-rtTA/TRE-Cre;$Erk1^{-/-}$;$Erk2^{lx/lx}$ called RPE-DKO, when injected with Dox (lane 3). (E) Cryostat section of fixed whole mount eyes, from CTL and RPE-DKO at 1 month, immunostained as indicated.(F) Western blot analysis of ERK1/2 expression in RPE protein lysates from CTL and RPE-DKO at 1 month; ARPE19 protein lysate is used as positive control for ERK1 expression.

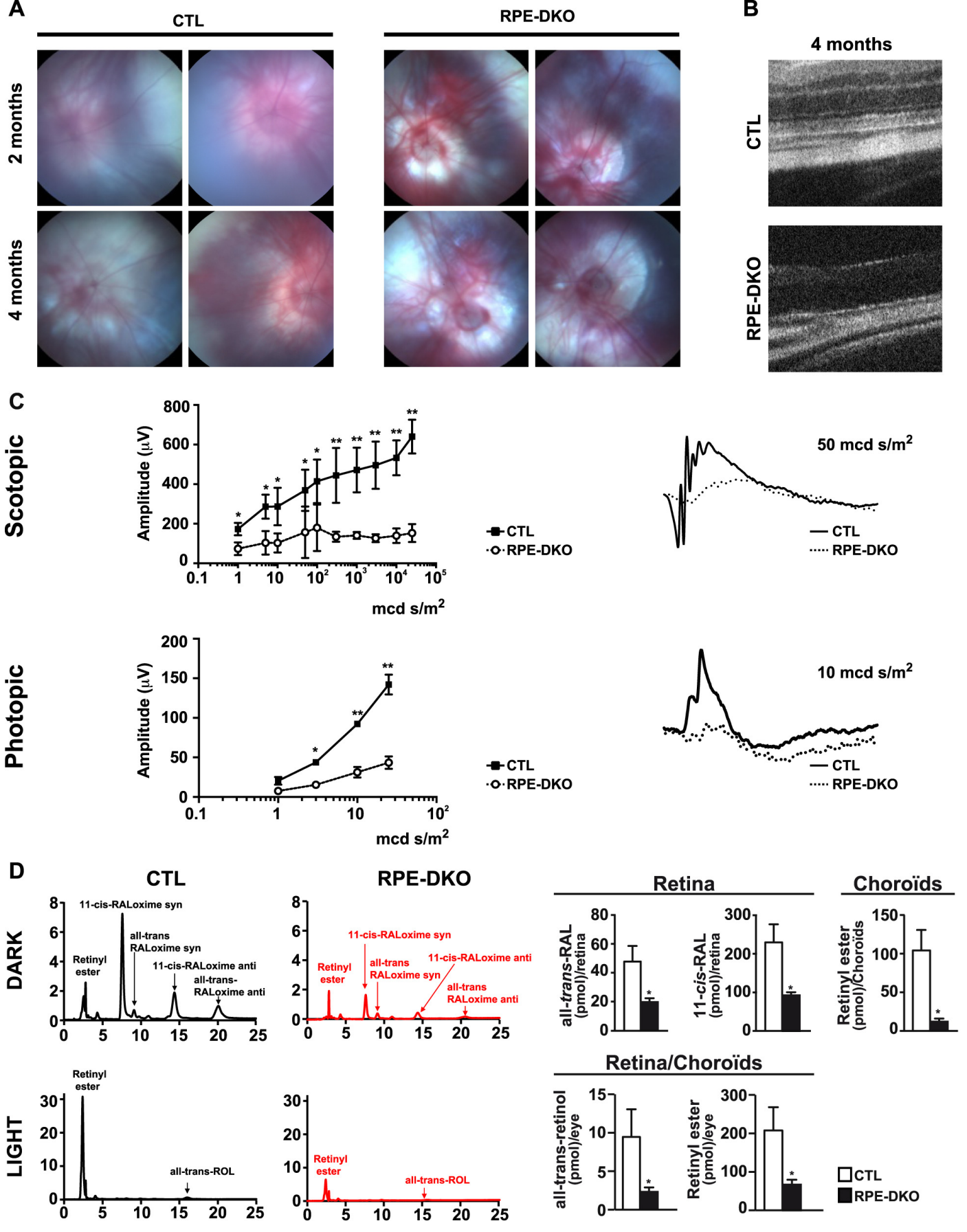

Fig. 2: Loss of ERK1/2 in RPE leads to vision impairment. (A) Representative fundus images of CTL and RPE-DKO at 2 or 4 months. (B) Representative OCT images of CTL and RPE-DKO at 4 months. (C) Graphs of the scotopic (n=10) and photopic (n=4) ERG response (b wave) taken in CTL and RPE-DKO at 2 months. (*p<0.05, **p<0.001). The right panel shows the scotopic (50 mcd s/m2) and the photopic (10 mcd s/m2) ERG response of CTL and RPE-DKO mice. (D) Chromatographs and quantification of retinoids measured in the retina and in the RPE/Choroid from mice at 1 month, dark-adapted for 16 hours or measured in whole eye (containing retina, RPE and choroid) from mice (same conditions) exposed to 1000 mA of light for 2 hours.

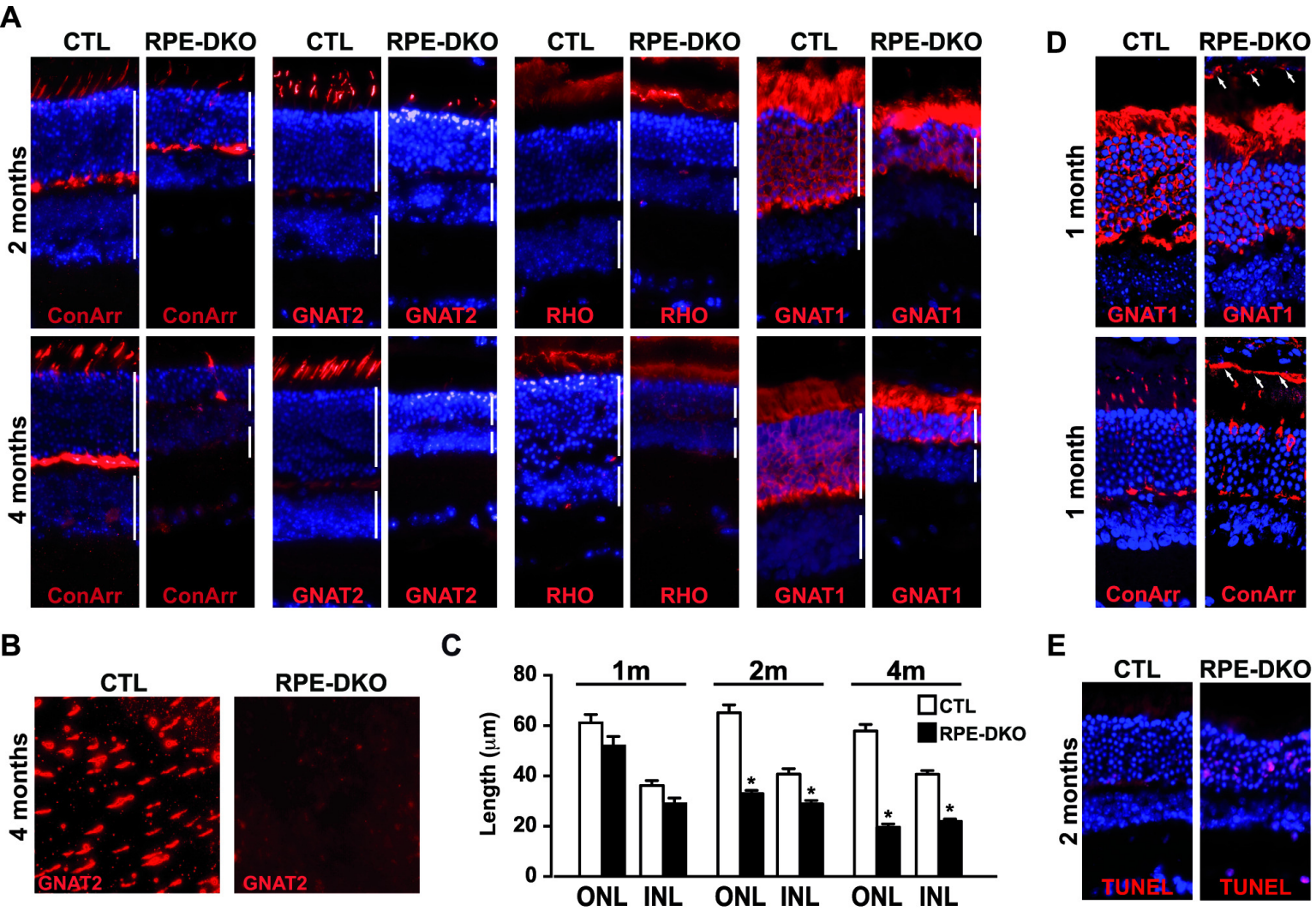

Fig. 3: Loss of ERK1/2 in RPE leads to photoreceptor degeneration. (A) Cryostat section of fixed whole mount eye, from CTL and RPE-DKO at 2 or 4 months, immunostained against different rods and cones markers as indicated. (B) Flatmount retinal preparation, from CTL and RPE-DKO at 4 months, immunostained as indicated. (C) Outer nuclear layer (ONL) and inner nuclear layer (INL) length measured manually using ImageJ. Data represent mean ± SEM of four independent experiments *p<0.05. (D) GNAT1 and ConeArrestin stainings from CTL and RPE-DKO at 1 month. Presence of both photoreceptor markers was observed in RPE of RPE-DKO mice (white arrows). (E) TUNEL staining of cryostat section of fixed whole mount eye from CTL and RPE-DKO at 2 months.

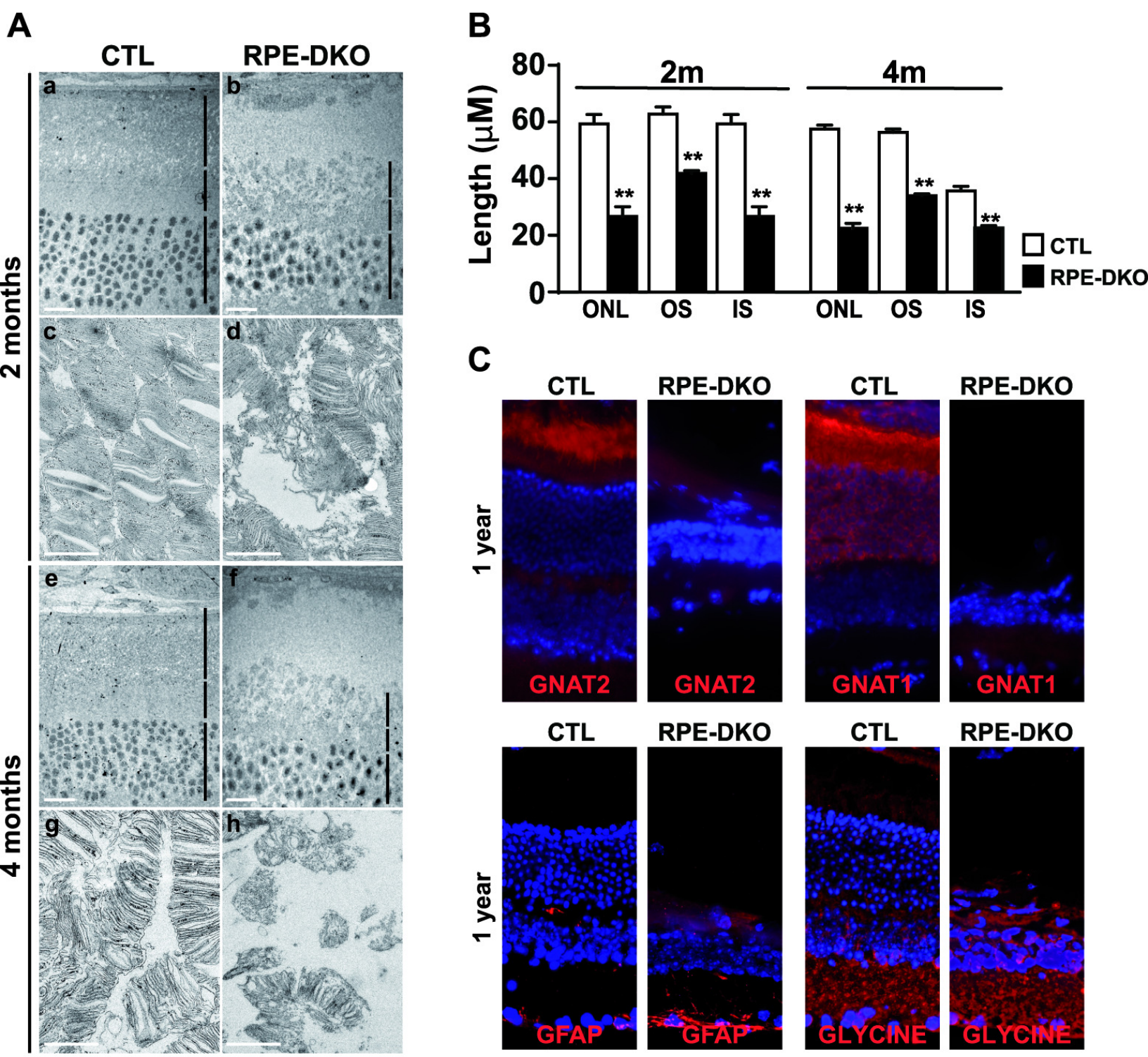

Fig. 4: Outer nuclear layer (ONL), outer segment (OS) and inner segment (IS) decrease during degeneration until to be completely absent in RPE-DKO at 1 year. (A) Electron microscopy images of retina-RPE layers from CTL and RPE-DKO at 2 or 4 months. The bottom panel is a magnification of outer segment (OS) layer of photoreceptors (PR). (B) Measurement of outer nuclear layer (ONL), outer segment (OS) and inner segment (IS) of the electron microscopy images. Data represent mean ± SEM of 3 experiments, **p<0.008. (C) Cryostat section of fixed whole mount eye, from CTL and RPE-DKO at 1 year, immunostained as indicated.

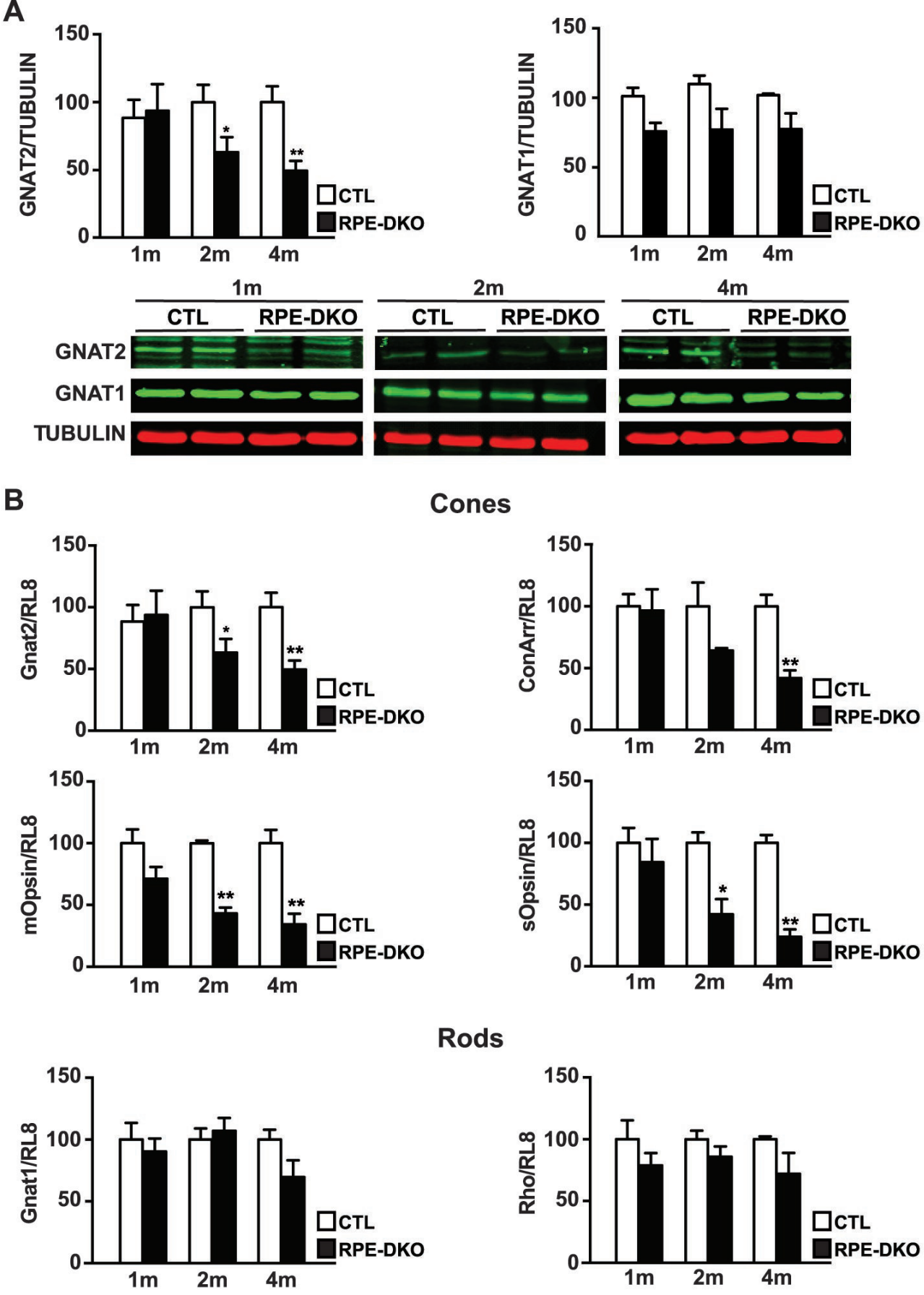

Fig. 5: Loss of ERK1/2 in RPE causes specific reduction in cone markers. (A) Representative images and quantification graphs of retinal protein lysates from CTL and RPE-DKO at 1, 2 or 4 months. Data represent mean ± SEM of 5 independent experiments (*p<0.02, **p<0.001). (B) Quantification graphs of QPCR performed on retinal extracts from CTL and RPE-DKO at 1, 2 or 4 months. RL8 was used as internal control to normalize RNA expression. Results are expressed as percent of CTL and as mean ± SEM of 4 independent experiments (*p<0.05, **p<0.003).

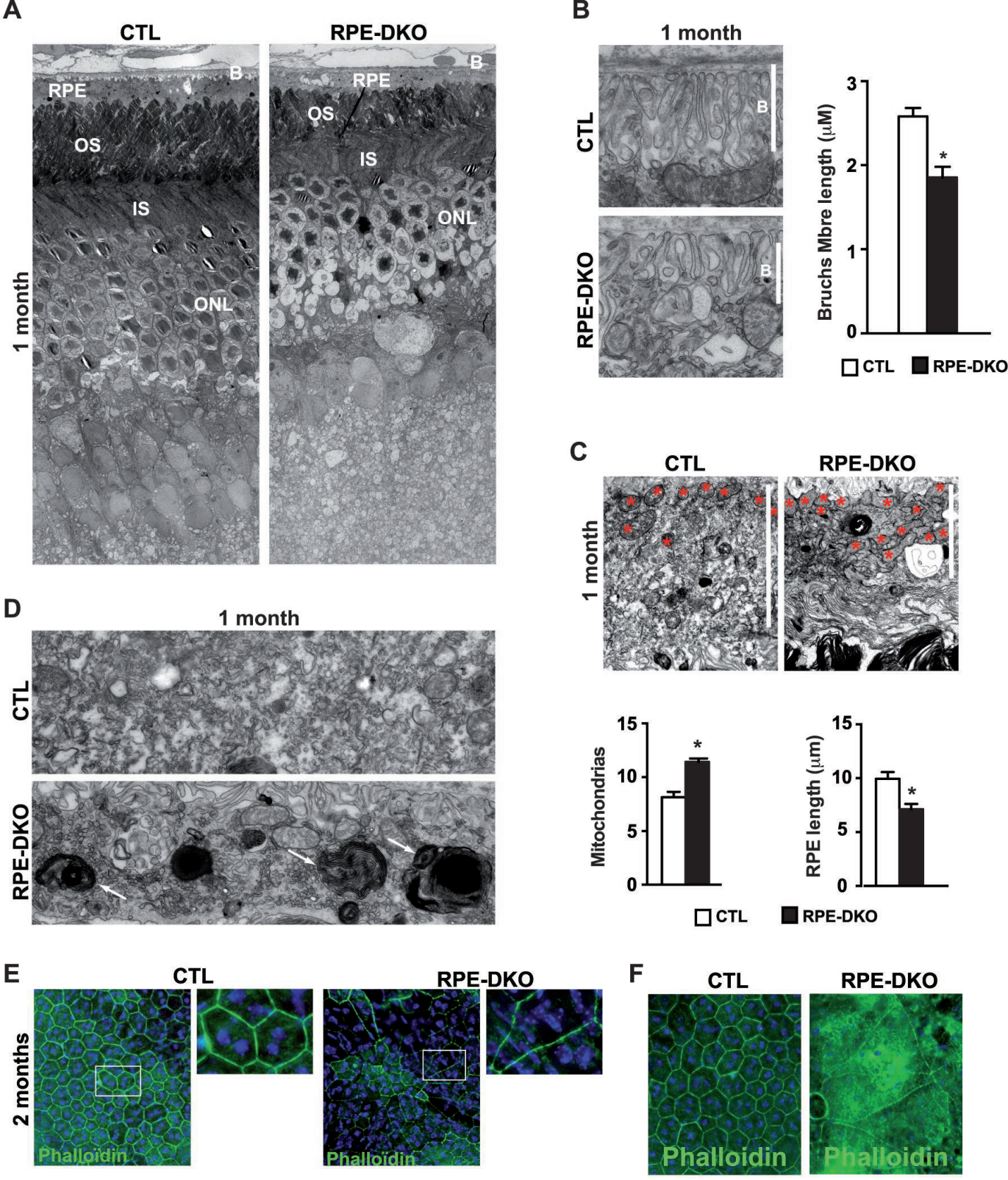

Fig. 6: Loss of ERK1/2 in RPE leads to massive ultrastructural changes in RPE-DKO at 1 month. (A) Representative electron microscopy images showing different retinal and RPE cell layers (B, Bruch's Membrane; RPE, Retinal Pigment Epithelium; OS, Outer Segment; IS, Inner Segment; ONL, Outer Nuclear Layer;). (B) Representative electron microscopy image of the Bruch's membrane (B, Bruch's membrane) and the underlying RPE cells and measurement of Bruch's membrane length (*p<0.0001). (C) Representative electron microscopy image of the RPE cell layer and the underlying OS of the PR and measurement of RPE length and quantification of the area of mitochondria (stars: mitochondria) (*p<0.015). (D) Electron microscopy image showing the accumulation of membrane-enriched phagolysosomes in the RPE of RPE-DKO in comparison to CTL (white arrows). (E and F) RPE flatmount from CTL and RPE-DKO at 2 months, immunostained against Phalloidin and counterstained with Dapi.

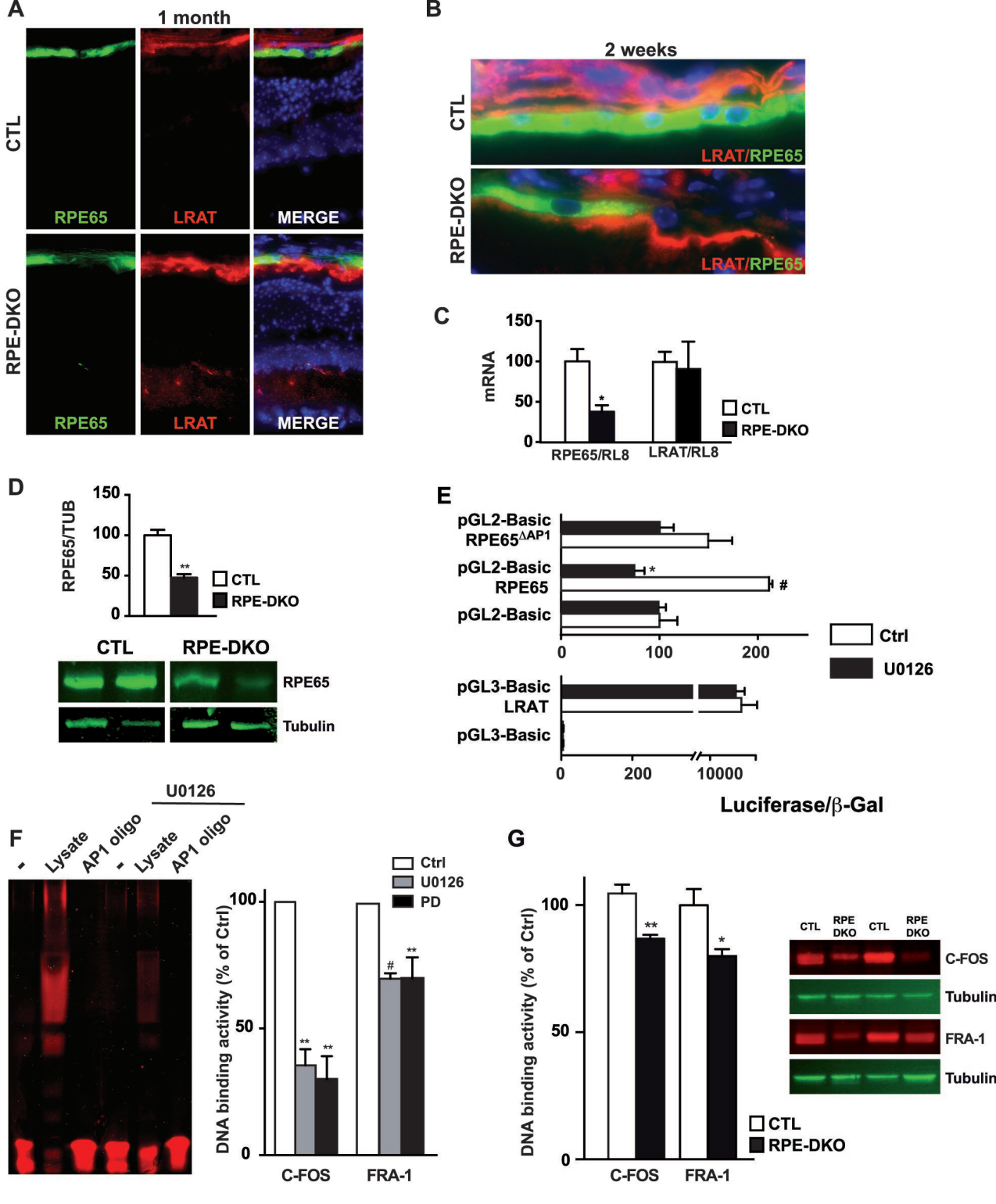

Fig. 7: ERK1/2 directly regulates RPE65 expression. (A) Cryostat section of fixed whole mount eyes, from CTL and RPE-DKO at 1 month, immunostained as indicated. (B) Cryostat section of fixed whole mount eyes, from CTL and RPE-DKO at 2 weeks, immunostained as indicated. (C) QPCR analysis of mRNA extracted from the RPE/choroid of CTL and RPE-DKO at 1 month, for the genes indicated. RL8 was used as internal control to normalize RNA expression. Results are expressed as percent of CTL and as mean ± SEM of 3 retinas, *p<0.03. (D) Representative immunoblot and quantification of RPE protein lysates from CTL and RPE-DKO at 1 month, immunoblotted as indicated, **p<0.0002, n=5. (E) Luciferase assay for both RPE65 and LRAT promoters. HEK293 cells were transfected and treated as indicated. The luciferase fluorescence was normalized to β-gal fluorescence. Data represent mean ± SEM of 4 independent experiments, *p<0.05 vs pGL2-Basic-RPE65, #p<0.05 vs pGL2-Basic. (F) EMSA assay of AP-1 complex in nucleus from ARPE19 cells treated or not with U0126. AP-1 DNA binding analysis from nuclear extract of ARPE19 cells treated either with U0126 or PD0325901. Data represent mean ± SEM of 3 independent experiments expressed as percent of control, *p<0.02, **p<0.002. (G) AP-1 DNA binding analysis of whole cell extracts from mice at 1 month. Data represent mean ± SEM of 3 independent experiments expressed as percent of control, *p<0.015, **p<0.002, n=6. Representative immunoblot of RPE protein lysates from CTL and RPE-DKO at 1 month, showing the expression of C-FOS and FRA-1; TUBULIN was used as control.

Table 1

The following primer sets were used:

Purpose	Genes		Primers
Genotype	Erk2	B	GCCTTCCAACCTCCTGCTGAACACC
		Wt	GCACCTAACAAAGCTTCACCCAGG
		D	AAGCTTGAGCTCCTCGAGAGATCGGC
		D1	GTACTGGATCCGAGCTCATAACTTCG
		D2	GGGATCAGCTTCAACCTTGCTGGG
	Erk1	A	GAAGGAGCCAAGCTGCTATT
		C	AGCAATGACCACATCTGCTA
		K	AACGTGTGGCTACGTACT
	Cre	R	CTAATCGCCATCTTCCAGCAGG
		F	AGGTGTAGAGAAGGCACTTAGC
	rTtA	R	TCAAACTCGAAGTCGGCCATATCC
		F	CGGCCTTGAATTGATCATATGCGG
QPCR	Gnat1	R	ACTGAATGTTGAGGTGGTC
		F	AGAGGATGCTGAGAAGGATG
	Gnat2	R	GACTTGAACTCTAGGCACTC
		F	CATCAGTGCTGAGGACAAAG
	sOpsin	R	AGGGCCAACTTTGCTAGAAG
		F	TGGTCAACAATCGGAACCAC
	mOpsin	R	GGCGCAGCTTCTTGAATCTC
		F	TGAGGATAGCACCCATGCAA
	Rpe65	R	AAAGCACAGGTGCCAAATTC
		F	CCCTCCTGCACAAGTTTGAC
	mRl8	R	GCTTCACTCGAGTCTTCTTG
		F	ACTGGACAGTTCGTGTACTG
	Lrat	R	GACAGCCGAAGCAAGACTGCT
		F	ACGCAGAGCTGAGCAGCAGTT
	ConeArr	R	AGTTGTCCAGACCACAGATG
		F	TTGTGCTAGAGGCCAGATTG